ORIGINAL ARTICLE

JBMR

CRELD2 Is a Novel LRP1 Chaperone That Regulates Noncanonical WNT Signaling in Skeletal Development

Ella P Dennis,[1] Sarah M Edwards,[2] Robert M Jackson,[1] Claire L Hartley,[2*] Dimitra Tsompani,[1] Mattia Capulli,[3] Anna Teti,[3] Raymond P Boot-Handford,[2] David A Young,[1] Katarzyna A Piróg,[1] and Michael D Briggs[1]

[1]Biosciences Institute, Newcastle University, International Centre for Life, Newcastle Upon Tyne, UK
[2]Wellcome Trust Centre for Cell-Matrix Research, University of Manchester, Manchester, UK
[3]Department of Biotechnological and Applied Clinical Sciences, University of L'Aquila, L'Aquila, Italy

ABSTRACT

Cysteine-rich with epidermal growth factor (EGF)-like domains 2 (CRELD2) is an endoplasmic reticulum (ER)-resident chaperone highly activated under ER stress in conditions such as chondrodysplasias; however, its role in healthy skeletal development is unknown. We show for the first time that cartilage-specific deletion of *Creld2* results in disrupted endochondral ossification and short limbed dwarfism, whereas deletion of *Creld2* in bone results in osteopenia, with a low bone density and altered trabecular architecture. Our study provides the first evidence that CRELD2 promotes the differentiation and maturation of skeletal cells by modulating noncanonical WNT4 signaling regulated by p38 MAPK. Furthermore, we show that CRELD2 is a novel chaperone for the receptor low-density lipoprotein receptor-related protein 1 (LRP1), promoting its transport to the cell surface, and that LRP1 directly regulates *WNT4* expression in chondrocytes through TGF-β1 signaling. Therefore, our data provide a novel link between an ER-resident chaperone and the essential WNT signaling pathways active during skeletal differentiation that could be applicable in other WNT-responsive tissues. © 2020 American Society for Bone and Mineral Research. © 2020 The Authors. *Journal of Bone and Mineral Research* published by American Society for Bone and Mineral Research..

KEY WORDS: CRELD2; WNT SIGNALING; SKELETAL DEVELOPMENT

Introduction

The endoplasmic reticulum (ER) is the largest organelle within the cell and predominantly functions as the site of protein synthesis and folding. Despite a wide range of ER-resident folding enzymes and chaperones, proteins can misfold and accumulate within the ER lumen, for instance due to high secretory load or the presence of pathological mutations. This triggers an evolutionarily conserved process called the unfolded protein response (UPR).

The UPR is initiated by the ER-resident chaperone BiP dissociating from its three transmembrane receptors, protein kinase RNA-like ER kinase (PERK), inositol-requiring enzyme 1 (IRE-1), and activating transcription factor 6 (ATF-6), and binding to exposed hydrophobic residues on the unfolded protein.[1] The UPR initially acts with the aim of decreasing protein translation, increasing refolding capacity, and degrading the misfolded protein; however, if the stress is not returned to physiological levels, the UPR can trigger cell death by inducing C/EBP homologous protein (CHOP)-dependent/−independent signaling cascades.[2,3]

Endochondral ossification is the process responsible for the development and postnatal growth of long bones and requires a cartilage precursor formed by chondrocytes. The cartilage growth plate, organized into three distinct chondrocyte differentiation zones—the resting, proliferative, and hypertrophic zones—drives long bone growth through a tightly regulated process involving proliferation, hypertrophy, mineralization, and apoptosis. Bone then forms on the cartilage scaffold and is continually remodeled throughout life through the combined actions of bone-forming osteoblasts and bone-resorbing osteoclasts. Interestingly, the UPR has also been implicated in the differentiation of these highly secretory skeletal cells. For example,

Received in original form January 10, 2020; revised form March 2, 2020; accepted March 10, 2020. Accepted manuscript online March 17, 2020.
Address correspondence to: Katarzyna A Piróg, DDS, and Michael D Briggs, PhD, Biosciences Institute, Newcastle University, International Centre for Life, Newcastle-upon-Tyne, NE1 3BZ, UK. E-mail: katarzyna.pirog@newcastle.ac.uk; michael.briggs@newcastle.ac.uk
Additional Supporting Information may be found in the online version of this article.
*Current address: Genomic Diagnostics Laboratory, Manchester Centre for Genomic Medicine, Central Manchester University Hospitals NHS Foundation Trust, Manchester, UK.
The peer review history for this article is available at https://publons.com/publon/10.1002/jbmr.4010.

Journal of Bone and Mineral Research, Vol. 00, No. 00, Month 2020, pp 1–18.
DOI: 10.1002/jbmr.4010

ATF4 is a transcription factor operating directly downstream of PERK; *Atf4*-null mice[4] have a skeletal dysplasia phenotype due to reduced chondrocyte differentiation and *Perk*-null mice[5] exhibit osteopenia due to impaired osteoblast maturation and activity.

The CRELD (cysteine rich with epidermal growth factor [EGF]-like domains) family of proteins comprises CRELD1 and CRELD2[6] and these are ER-localized[7] multidomain proteins composed of EGF-like and calcium-binding EGF-like repeats and a unique and highly conserved tryptophan-aspartic acid (WE)[8] domain. During embryogenesis, CRELD1 is expressed in various soft tissues and has been shown to play a crucial role in heart development with *CRELD1* mutations associated with atrioventricular septal defects.[9] CRELD2 is expressed in the developing skeleton as well as several soft tissues and to date five human isoforms,[8] comprising varying numbers of EGF-like domains, have been identified. In contrast, only one CRELD2 isoform, homologous to the CRELD2α human isoform, has been identified in mice. The precise function of CRELD2 is largely unknown; however, CRELD2β has been shown to bind to and be involved in the folding of the nicotinic acetylcholine receptor α4 and β2 subunits.[10] CRELD2 was first identified as an ER stress-inducible gene after treatment of neuro2α cells with thapsigargin[7] and importantly, the promoter of *CRELD2* contains an AFT6 response element.[7] Unlike CRELD1, which is anchored by two C-terminal type II transmembrane domains,[6] CRELD2 has been shown to be secreted during ER-stress[11,12] suggesting a functional divergence between the two family members. The four C-terminal amino acids (REDL), comprising an imperfect C-terminal KDEL ER-retention sequence, play an important role in the secretion of CRELD2 that is further enhanced by BiP[11] and MANF[13]; however, its exact role outside of the cell is currently unknown.[7]

Several studies have implicated CRELD2 in the pathobiology of ER-stress-mediated conditions such as kidney disease[14] and aortic aneurysm in Marfan syndrome.[15] *Creld2* is also upregulated and secreted in mouse models of multiple epiphyseal dysplasia[16] and metaphyseal chondrodysplasia type Schmid,[17] skeletal dysplasias characterized by the retention of mutant proteins in the ER of chondrocytes that results in prolonged ER stress. Substrate-trapping experiments have shown that CRELD2 acts as a putative protein disulphide isomerase (PDI)[12] for substrates such as matrilin-3, laminin 5 β3, type VI collagen, and thrombospondin 1. Moreover, CRELD2 is upregulated in BMP9 stimulated osteogenic differentiation of mesenchymal stem cells (MSCs) through SMAD1/6/5 binding directly to its promoter, suggesting a novel role for CRELD2 in bone development.[18]

Despite these indications, the role of CRELD2 in skeletal development and homeostasis is not clearly understood. We therefore generated and studied in depth cartilage-specific and bone-specific *Creld2* knockout mouse models to investigate the role of CRELD2 in skeletal development and homeostasis.

Materials and Methods

Generation of *Creld2* conditional knockout mice

A *Creld2* gene trap (Creld2$^{tm1b(EUCOMM)Hmgu}$) targeting vector containing a large selection cassette was obtained from the European Conditional Mouse Mutagenesis Programme (EUCOMM), electroporated into C57BL6 blastocysts, and used to generate chimeras that were bred onto the C57BL6 background (Supplemental Fig. S1*A*). The introduction of this large targeting vector did not abolish CRELD2 expression as identified by Western blotting of liver tissue (Supplemental Fig. S1*B*). Therefore, mice heterozygous for the targeted allele were crossed with *Actin-flp* mice generating offspring with the conditional *Creld2* allele, which was identified by genomic DNA PCR using the primers 5′-GGT GGA CAC CTG TCA ATG GT-3′ and 5′-CAG CAT GAG AAA GGG AGC TTA-3′ (Supplemental Fig. S1*C*). These mice were then bred with mice expressing the *Cre* transgene under type II collagen (*Col2a1*) promoter to generate *Creld2* cartilage-specific knockout mice (*Creld2*$^{CartΔex3–5}$) and under osteocalcin (*Bglap*) promoter to generate bone-specific (*Creld2*$^{BoneΔex3–5}$) knockout mice by Cre recombination, resulting in the deletion of exons 3–5 of *Creld2*. Mice with the conditional *Creld2* allele were also crossed with global deleter *Cre* mice, and Western blotting of liver tissue was used to confirm that CRELD2 expression was abolished by *Cre* recombination (Supplemental Fig. S1*D*). The presence of the *Cre* transgene in the conditional lines was identified by genomic DNA PCR using the primers 5′-TGC CAC CAG CCA GCT ATC AAC T-3′ and 5′-AGC CAC CAG CTT GCA TGA TCT C-3′ (Supplemental Fig. S1*E*). RT-PCR was performed to confirm the deletion of *Creld2* in chondrocytes and osteoblasts (Supplemental Fig. S1*F*). All experiments were carried out in compliance with the Animals Scientific Procedures Act 1986 according to Directive 2010/63/EU of the European Parliament, under project license PPL60/4525.

X-ray and micro-computed tomography (μCT)

X-ray images were obtained using the MX-20 Cabinet X-ray System (Faxitron, Tucson, AZ, USA). Bone measurements were taken at 3, 6, and 9 weeks of age using the image processing program FIJI (ImageJ).[19] To analyze bone structure, undecalcified bone samples fixed in 4% paraformaldehyde (PFA) were subjected to μCT analysis using the SkyScan 1174v2 (Bruker, Kontich, Belgium) μCT device. Multiple 2D image projections were acquired at 50 kV and 800 mA with a resolution of 6.74 nm. Image reconstruction was carried out using the SkyScan NRecon program. Common standard 3D bone morphometric parameters were determined for trabecular and cortical bone using the CTAn program.[20] Trabecular bone architecture was calculated from 350 serial slides of 6 microns thick, 650 μm from the growth plate. Cortical bone architecture was calculated from 100 serial slides of 6 microns thick, 3.5 mm from the growth plate.

Histological and immunohistochemical staining of cartilage

Cartilage samples were fixed for histology and immunohistochemistry and processed as outlined previously.[21] Formalin-fixed sections were stained with hematoxylin and eosin (H&E) and toluidine blue. For immunohistochemistry (IHC), antigen retrieval was performed by incubation in 0.2% bovine hyaluronidase, 0.2% Triton-X, and 20 μg/mL proteinase K. Sections were blocked in serum for 1 hour, incubated in primary antibody overnight at 4 °C, and probed with the appropriate secondary antibody for 1 hour at room temperature. Sections were mounted in Fluoroshield mounting media with DAPI (Abcam, Cambridge, UK). The following primary antibodies were used: acetylated-tubulin (ab24610), collagen I (ab34710), collagen II (ab34712) (all from Abcam), CRELD2 (sc86110, Santa Cruz Biotechnology, Dallas, TX, USA), matrilin-3 (AF3357, R&D Systems, Minneapolis, MN, USA), aggrecan (Professor Tim Hardingham, The University of Manchester), and collagen X (Professor Karl Kadler, The University of Manchester). Negative controls are shown in Supplemental Fig. S2*F*. To analyze chondrocyte proliferation, 3-week-

old mice were injected subcutaneously with BrdU labeling reagent according to weight (0.1 mg per 10 g). Two hours after injection, mice were euthanized and limbs harvested. IHC was then performed to detect BrdU-positive cells using an anti-BrdU antibody (ab6326, Abcam). BrdU-positive cells in the proliferative zone of the growth plate were counted using the watershed algorithm in the FIJI program and expressed as a percentage of the total number of osteoblasts or the total number of chondrocytes within the proliferative zone. Analysis was performed on three matched slides per mouse from three mice per genotype.

TUNEL analysis

Cell death was detected by fragmented DNA and quantified using the DeadEND Fluorometric TUNEL System (Promega, Madison, WI, USA) according to manufacturer's instructions. Permeabilization was performed by boiling samples in citric buffer pH 6 as Proteinase K treatment can generate false positives.[22] TUNEL-positive cells were counted using the watershed algorithm in FIJI and were expressed as a percentage of the total number of osteoblasts or the total number of chondrocytes within each zone of the growth plate. Analysis was performed on three matched slides per mouse from three mice per genotype.

Transmission electron microscopy (TEM)

Tibial cartilage from 1-week-old pups was dissected and fixed in 2% glutaraldehyde in 0.1 M sodium cacodylate buffer at 4°C. Samples were then processed, embedded, and sectioned by the Electron Microscopy Research Services Unit at Newcastle University. The protocol was as follows. Cartilage samples were then washed three times in 0.1 M sodium cacodylate and fixed a second time in 2% (w/v) osmium tetroxide in distilled water. Tissues were then rinsed twice in water, immersed in 2% uranyl acetate, and rinsed twice again in water before being washed with 25%, 50%, 75% acetone. Samples were then incubated in two changes of 100% acetone and embedded using the TAAB epoxy resin kit according to manufacturer's specification. To allow for resin to fully penetrate the tissues, samples were incubated in 100% resin for 2 days. Tibial cartilage samples were then placed in a mold and resin was polymerized overnight at 60°C. After embedding, samples were sectioned to ultrathin sections of 70 nm using a diamond knife on a Leica (Buffalo Grove, IL, USA) EM UC7 ultramicrotome, stretched with chloroform and mounted onto Pioloform-filmed copper grids. Prepared grids were then stained with 2% aqueous uranyl acetate and lead citrate solution. Prepared grids were imaged using the Phillips CM100 Transmission Electron Microscope.

Bone histomorphometry

Nine-week-old tibias were dissected and fixed in 4% formaldehyde for 24 hours and embedded in methylmethacrylate without decalcification. Sections (6 μm) were stained with Von Kossa (to analyze calcification), 1% toluidine blue (to analyze osteoblast number[23]), and stained for TRAcP (to analyze osteoclast number and surface[23]). To study the dynamic parameters of bone, mice were injected in the intraperitoneal cavity 1 week and 1 day before euthanization with 30 mg/kg alizarin complexone and 20 mg/kg calcein in a 2% sodium bicarbonate pH 7.4 solution, respectively. Trabecular bone histomorphometric measurements were performed on 6-μm-thick sections from fluorescent images acquired using a Zeiss (Thornwood, NY, USA) Axio imager 2 microscope. The analysis of the bone formation rate (BFR)[23] was carried out on matched sections from 5 mice per genotype and was performed on the trabecular bone in the proximal tibia, 100 μm below the growth plate.

Primary cell extraction and cell culture

MSCs were isolated from bone marrow aspirates, cultured and phenotyped as previously described.[24,25] Primary chondrocytes were isolated after digestion of 5-day-old costal and tibial cartilage with 2.5 mg/mL collagenase IA as outlined previously.[21] Primary chondrocytes were cultured for up to 7 days in complete DMEM/F-12 (supplemented with 10% FBS, 5% non-essential amino acids, 1 U/mL penicillin, 1 μg/mL streptomycin, and 50 μg/mL L-ascorbate-2-phosphate). Primary osteoblasts were isolated from 1-week-old neonatal calvarias by sequential enzymatic digestion of the bone matrix.[26] Cells released in the second and third digestion were pelleted by centrifugation and cultured in complete alpha MEM (supplemented with 10% FBS, 1 U/mL penicillin, and 1 μg/mL streptomycin). To generate mature osteoblasts, primary osteoblasts were cultured for 21 days in osteogenic media (complete alpha MEM containing 50 μg/mL L-ascorbate-2-phosphate, 10 mM β-glycerophosphate, and 0.1 μM dexamethasone). Osteoclast precursors were isolated from the long bones of 6- to 9-day-old mice.[27] The bone marrow mononuclear cell fraction was obtained by centrifugation of Histopaque-1077. Cells were plated in 12-well plates and cultured for 48 hours in complete alpha MEM containing 30 ng/mL M-CSF (R&D Systems) generating M-CSF-dependent macrophages. Osteoclastogenesis was performed by culturing macrophages for 1 week in complete alpha MEM supplemented with 30 ng/mL M-CSF and 100 ng/mL RANKL (R&D Systems). Osteoclastogenesis media was refreshed every 2 days. To analyze the effect of wild-type and *Creld2* knockout primary osteoblast conditioned media, osteoclastogenesis was performed in conditioned media. The SW1353 chondrocyte-like and the SAOS2 osteoblast-like cell lines were maintained in complete DMEM/F-12 and complete alpha MEM, respectively. For WNT4 stimulation studies, recombinant WNT4 (R&D Systems) was added at a concentration of 100 ng/mL. For TGFβ1 stimulation studies, recombinant TGFβ1 (R&D Systems) was added at a concentration of 5 ng/mL.

Protein extraction and immunoblotting

Protein lysates were extracted as outlined previously.[21] Protein concentrations were obtained using the Pierce (Rockford, IL, USA) BCA kit. Samples were denatured by boiling and reduced by DTT where appropriate. For analysis of plasma membrane protein expression, plasma membranes were extracted using the plasma membrane protein extraction kit from Abcam. Western blotting was performed as outlined previously.[21] The following primary antibodies were used: p38 (ab170099), Phospho p38 (T180 + Y182) (ab195049), β-catenin (ab32572), osteoprotegerin (ab183910), LRP1 β-chain (ab92544), alpha 1 sodium potassium ATPase antibody (ab7671) (all from Abcam), GAPDH (Millipore, Burlington, MA, USA), and CRELD2 and RANKL (sc377079, Santa Cruz). Membranes were imaged on the LI-COR Odyssey CLx Imaging System. Densitometric analysis of the fluorescent protein bands was presented relative to protein loading or GAPDH levels. Analysis was performed on three samples per condition.

Enzyme-linked immunosorbent assay (ELISA)

To determine the concentration of secreted RANKL and OPG in osteoblast conditioned media, media was concentrated using the Vivaspin 15 MWCO centrifugal concentrators for 30 minutes at 15,000*g*. The mouse RANKL and mouse Osteoprotegerin Quantikine ELISA kits from R&D systems were then used to determine protein concentration in the concentrated conditioned media as outlined in the manufacturer's instructions.

RNA extraction and sequencing

RNA was extracted from whole knee joint cartilage of 5-day-old mice using the Promega Reliaprep RNA Tissue Miniprep System as outlined previously.[21] RNA was also extracted from cells using the Promega Reliaprep RNA Cell Miniprep System according to the manufacturer's protocol. The extracted RNA from cartilage knee joints and primary osteoblasts were sent to GATC Biotech for RNAseq analysis. Each of the three samples contained two individually extracted RNA samples, pooled into one sample at a concentration of 1 μg RNA with a RIN >8. The RNA was sequenced and analyzed by GATC Biotech. Briefly, Bowtie was used to align the RNA sequencing reads to the mouse reference genome. TopHat, Cufflinks, and Cuffmerge were used to identify exon-exon splice junctions, and identify, quantify, and annotate the processed RNA-sequencing alignment assembly. Cuffdiff was then used to determine differential expression levels of wild-type and knockout merged transcripts. Several RNA-sequencing hits were confirmed by quantitative-PCR (qPCR).

Quantitative-PCR (qPCR)

cDNA was synthesized from RNA using the GoScript Reverse Transcription System according to the manufacturer's protocol. RNA was removed after the incubation with 1 U RNase H for 20 minutes at 37°C. qPCR was performed using the Power SYBR Green method as outlined in the manufacturer's instructions on a Bio-Rad (Hercules, CA, USA) DNA engine Peltier Thermal Cycler. For primer sequences, see Supplemental Table S7. Samples were analyzed in duplicate on each plate and the level of cDNA was normalized to the level of *18S*. qPCR results presented in Fig. 4 were obtained by TaqMan real-time PCR as described previously.[25] Sequences for TaqMan qPCR primers and corresponding Universal Probe Library (UPL) probes are outlined in Supplemental Table S8.

siRNA gene silencing

For siRNA transfection, 100 nM SMARTpool ON-TARGETplus siRNA of four specific siRNA duplexes were used to target *CRELD2* (L-010856, Horizon, Dharmacon, Lafayette, CO, USA) and *LRP1* (L-004721, Horizon, Dharmacon*)*. This was transfected into cells using the Dharmafect transfection reagent 1 (Horizon, Dharmacon). Reduction of gene-specific mRNA levels was calculated by comparing levels on cells transfected with 100 nM siCONTROL non-targetting siRNA (D-001206-14). For chondrogenesis, MSCs were transfected once before the induction of chondrogenesis. For osteogenesis experiments, MSCs in monolayer were transfected every week with siRNA for the duration of the experiment.

MSC differentiation and validation

For chondrogenesis, MSCs were cultured as a pellet in chondrogenic medium (DMEM supplemented with 1 U/mL penicillin, 1 μg/mL streptomycin, 100 μg/mL sodium pyruvate, 100 nM dexamethasone, 50 μg/mL L-ascorbate-2-phosphate, 1X ITS-1 premix, 10 ng/mL TGFβ3). For histology, either 500,000 (large) or 100,000 (mini) MSCs were seeded into a pellet. For gene expression analysis, 150,000 MSCs were seeded into a pellet. Chondrogenic media was replaced every 2 to 3 days for 14 days. For osteogenesis, MSCs were seeded in monolayer and induced to differentiate in osteogenic media as outlined above. Osteogenic media was replaced every 2 to 3 days for 21 days. For WNT4 recovery studies, recombinant WNT4 (R&D Systems) was added at a concentration of 100 ng/mL and was added to the culture from day 4 (chondrogenesis) and day 7 (osteogenesis).

Analysis of osteoblast differentiation and activity in vitro

Alizarin Red S staining was performed on mature osteoblast monolayers to analyze mineralization. Briefly, monolayers were fixed in 4% PFA and stained with 40 mM Alizarin Red S for 30 minutes. Staining intensity was calculated relative to Alizarin Red S standards at a wavelength of 405 nm. Alkaline phosphatase activity was determined on mature osteoblast protein lysates using the alkaline phosphatase colorimetric assay kit from Abcam. Analysis was performed on three samples per condition.

Co-immunoprecipitation and mass spectrometry

A previously generated V5-tagged wild-type CRELD2 cDNA construct in pcDNA 3.1 (+)[12] was used to overexpress CRELD2 in the chondrocyte-like SW1353 and osteoblast-like SAOS2 cell lines. To assess the binding partners of CRELD2, protein–protein interactions were cross-linked by incubation in 1.0 mM DSP for 10 minutes at room temperature. The reaction was stopped upon the addition of Tris-HCl pH 7.5 added to a final concentration of 20 mM for 15 minutes at room temperature. Cellular proteins were harvested and clarified by centrifugation at 10,000*g*. Lysates were precleared with 5% (v/v) protein A Sepharose for 30 minutes at 4°C with gentle rotation. Protein lysate (500 μg) was added to the anti-V5 agarose beads and incubated overnight at 4°C under gentle rotation. CRELD2 interacting proteins were identified by LC/MS-MS performed by the Mass Spectrometry Facility at The University of Manchester.

Immunocytochemistry

To assess the intracellular localization of CRELD2, primary chondrocytes were fixed in 10% formalin for 10 minutes at room temperature. Plasma membranes were labeled with wheat germ agglutinin (WGA) AlexaFluor 594 conjugate. Cells were then permeabilized for 5 minutes in 0.5% Triton-X before immunolabeling. The following primary antibodies were used: CRELD2, GRP94 (sc1794, Santa Cruz), GLG1 (AF7879, Biotechne), and EEA1 (AF8047, R&D Systems). For labeling of membrane LRP1, living cells were incubated for 2 hours at 37°C in a primary antibody raised against LRP-1 clone 8G1 that detects the extracellular LRP1 α-chain (Abcam). The cells were washed three times in PBS and incubated in an anti-mouse secondary antibody labeled with AlexaFluor 488 for 20 minutes at 13°C. Cells were then fixed in 10% formalin for 10 minutes at room temperature. Immunocytochemistry slides were mounted in Fluoroshield mounting media with DAPI and images were acquired at ×630 magnification using a Nikon (Tokyo, Japan) A1R confocal microscope.

Statistics

Results are expressed as the mean ± the standard deviation (SD) of a minimum of three individual experiments/mice.

Statistical significance was analyzed by Student's unpaired *t* test, and statistical significance was $p < 0.05$.

Results

The ablation of *Creld2* impairs skeletal development

To study the role of CRELD2 specifically in cartilage and bone development, we generated *Creld2* conditional knockout mouse models (Supplemental Fig. S1).

Interestingly, cartilage-specific *Creld2* knockout mice (*Creld2*-$^{Cart\Delta Ex3-5}$) displayed a chondrodysplasia-like phenotype with disproportionate short stature due to impaired endochondral ossification (Fig. 1*A*). For example, the long bones of *Creld2*-$^{Cart\Delta Ex3-5}$ mice were significantly shorter than controls and they also displayed reduced bone density with disrupted trabecular bone architecture (Fig. 1*B*). In contrast, intramembranous ossification of the cranial bones, measured by the inner canthal distance (ICD), was unaffected. Hematoxylin and eosin (H&E) staining of cartilage growth plate sections from 3-week-old *Creld2*$^{Cart\Delta Ex3-5}$ mice revealed a disrupted growth plate with numerous areas of hypocellularity and an overall reduction in the number of chondrocytes within individual growth plate zones (Fig. 1*C*).

Disruptions to primary cilia length and orientation result in growth plate defects and lead to cell misalignment[28] and abnormal cell morphology. It has been suggested that the columnar organization of chondrocytes within the proliferative zone may be controlled by primary cilia that normally align in an axis parallel to bone growth.[29] Interestingly, the proliferative zone of *Creld2*$^{Cart\Delta Ex3-5}$ growth plates lacked the typical columnar organization observed in controls, and primary cilia in the mutant mice were no longer aligned in an axis parallel to bone growth[29] (Fig. 1*C* and Supplemental Fig. S2*B*). In the hypertrophic zone, matrix mineralization creates a hypoxic environment depleted of nutrients and results in chondrocyte death. Whereas the late hypertrophic zone of growth plates in control mice were characterized by cellular debris, in *Creld2*$^{Cart\Delta Ex3-5}$ mice, chondrocytes were present within the newly ossified bone (Fig. 1*C*) and displayed an abnormal morphology that was more indicative of elliptical-looking proliferative chondrocytes (Supplemental Fig. S2*A*). Additionally, the height of the zone of type X collagen expression (a marker of chondrocyte hypertrophy) was significantly reduced in the *Creld2*-null growth plates, suggesting a decrease in numbers of mature hypertrophic chondrocytes (Fig. 1*D*). In contrast, the expression of other cartilage extracellular matrix proteins was unaffected (Supplemental Fig. S2*C*). Consistent with changes observed in other mouse models of human growth plate dysplasias,[16,30,31] moreover, the deletion of *Creld2* in chondrocytes significantly reduced cell proliferation and increased apoptosis (Fig. 1*E*). Thus, we conclude that *Creld2* ablation in chondrocytes impairs endochondral ossification by disrupting chondrocyte maturation and survival within the growth plate.

The ablation of *Creld2* impairs bone homeostasis

Interestingly, the bone-specific *Creld2* knockout mice (*Creld2*$^{Bone\Delta Ex3-5}$) demonstrated growth retardation (Fig. 2*A*) and showed an osteopenic phenotype characterized by significantly reduced bone mass with altered trabecular and cortical architecture (Fig. 2*B*). Toluidine blue staining revealed significantly less mature bone-forming osteoblasts and osteocytes in *Creld2*$^{Bone\Delta Ex3-5}$ mice compared with controls (Fig. 2*C*). Furthermore, deletion of *Creld2* in mature osteoblasts resulted in increased osteoblast apoptosis in vitro (Fig. 2*D*) and a reduction in the rate of bone formation as demonstrated by dynamic histomorphometry (Fig. 2*E*). In addition, there was also a significant increase in the osteoclast number and the erosion surface in *Creld2*$^{Bone\Delta Ex3-5}$ bones as identified by staining for the osteoclast marker tartrate-resistant acid phosphatase (TRAcP) (Supplemental Fig. S3*A*).

The cross-talk between osteoblasts and osteoclasts is central to maintaining bone homeostasis. Therefore, we next measured the expression of the osteoclastogenic cytokine receptor activator of nuclear factor kappa-B ligand (RANKL) and its decoy receptor osteoprotegerin (OPG) that inhibits osteoclastogenesis. The RANKL/OPG axis was disrupted at both the RNA and protein level in osteoblasts from *Creld2*$^{Bone\Delta Ex3-5}$ mice. RANKL expression at both the gene (*Tnfsf11*) and protein level was upregulated in *Creld2*$^{Bone\Delta Ex3-5}$ osteoblasts; however, OPG expression at the gene (*Tnfrsf11b*) and protein level was unchanged (Supplemental Fig. S3*B*). Additionally, the levels of secreted RANKL were significantly increased in media collected from *Creld2*$^{Bone\Delta Ex3-5}$ osteoblasts in vitro, whereas the secretion of OPG was increased (Supplemental Fig. S3*C*). Overall these data suggested that the upregulation of RANKL expression could result in the significant increase in osteoclast number in *Creld2*$^{Bone\Delta Ex3-5}$ mice. To verify whether the impaired RANKL/OPG ratio in *Creld2*$^{Bone\Delta Ex3-5}$ osteoblasts stimulated osteoclastogenesis, we differentiated pre-osteoclasts in vitro in conditioned media from the osteoblasts of *Creld2*$^{Bone\Delta Ex3-5}$ and control mice. The levels of several osteoclast markers (*Acp5*, *Calcr*, and *Ctsk*) were significantly upregulated in primary osteoclasts differentiated in *Creld2*$^{Bone\Delta Ex3-5}$ conditioned media, indicating that disrupted RANKL/OPG axis promotes osteoclast formation (Supplemental Fig. S3*D*). Thus, we conclude that CRELD2 deficiency in mature osteoblasts impairs bone homeostasis by impairing osteoblast maturation, activity, and survival and by disrupting osteoblast/osteoclast cross-talk.

The deletion of *Creld2* disrupts WNT signaling

To further assess the effect of CRELD2 deletion on chondrogenesis and osteogenesis, we analyzed the global gene expression profiles of both *Creld2* knockout chondrocytes and mature osteoblasts by RNA-sequencing. After the ablation of *Creld2*, 220 genes were differentially expressed in chondrocytes (Fig. 3*A*) compared with 1021 in osteoblasts (Fig. 3*B*). The enriched Gene Ontology (GO) term clusters for the differentially expressed genes in *Creld2*$^{Cart\Delta Ex3-5}$ chondrocytes (Supplemental Table Table S1) and *Creld2*$^{Bone\Delta Ex3-5}$ mature osteoblasts (Supplemental Table S2) comprised genes with ubiquitous cellular function and genes related to skeletal development and ossification. Of particular note, genes involved in cell cycle arrest, apoptosis, and embryonic skeletal system development were differentially expressed in *Creld2*$^{Cart\Delta Ex3-5}$ chondrocytes. The expression of several key genes was verified by qPCR (Fig. 3*C*). For example, *Mmp13* encoding a matrix metalloproteinase and a marker of chondrocyte hypertrophy[32] was significantly downregulated in *Creld2*$^{Cart\Delta Ex3-5}$ chondrocytes. Additionally, the expression of *Cyr61*, encoding Cysteine-rich protein 61 that promotes chondrogenesis in vitro,[33] was also downregulated in *Creld2*$^{Cart\Delta Ex3-5}$ mice. Similar to the GO clusters from *Creld2*$^{Cart\Delta Ex3-5}$ chondrocytes, differentially expressed genes in *Creld2*$^{Bone\Delta Ex3-5}$ mature osteoblasts clustered into genes

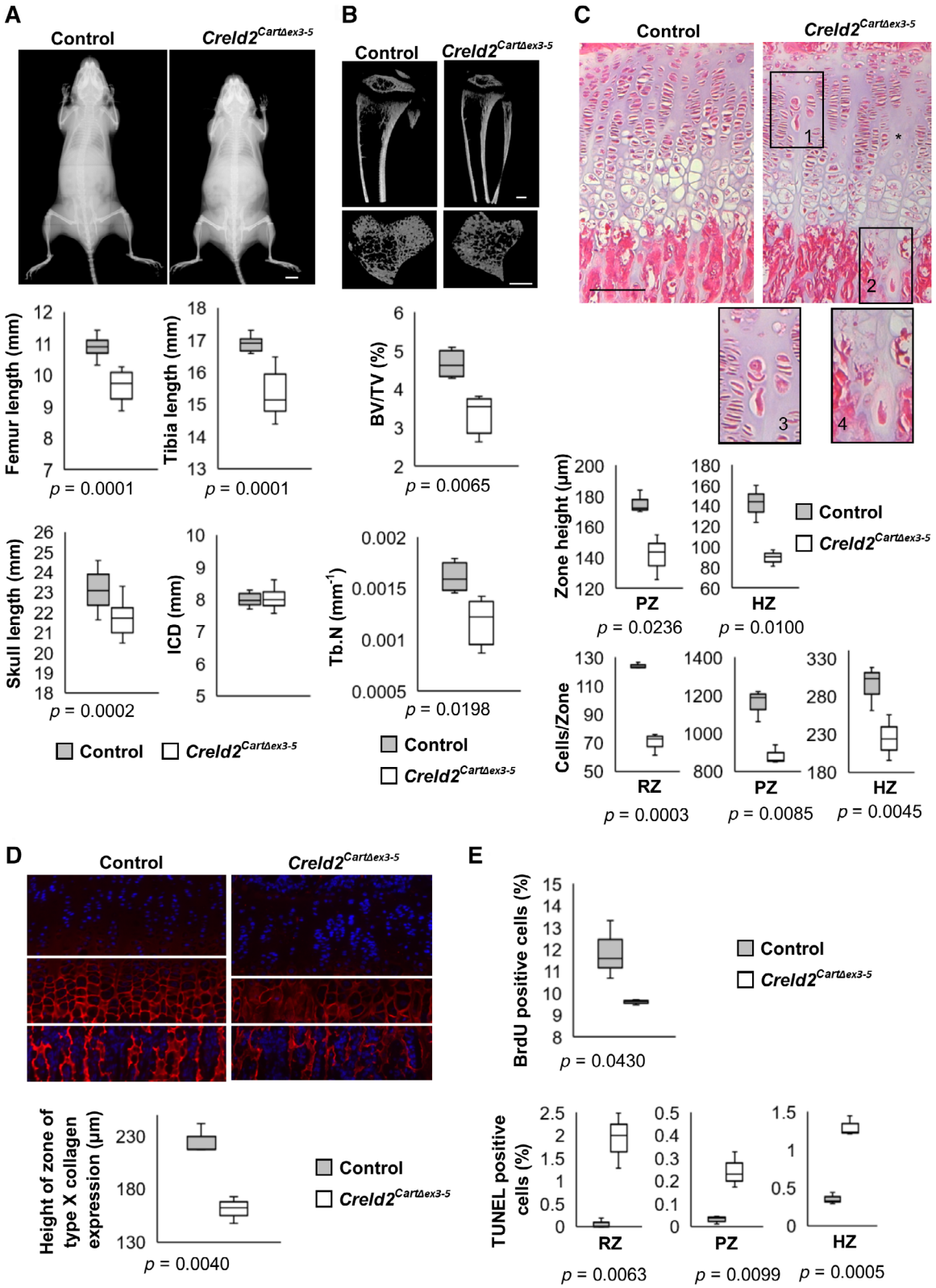

Fig. 1. *Creld2*$^{CartΔEx3–5}$ display a chondrodysplasia phenotype with a disrupted epiphyseal growth plate due to impaired chondrocyte maturation and survival. (*A*) Representative X-ray images at age 9 weeks and bone measurements showing a defect in endochondral ossification. Scale bar = 5 mm. (n = >10 per genotype.) (*B*) Bone microarchitecture analysis at age 9 weeks from μCT (representative images of sagittal and transverse projection). Scale bar = 500 μm. n = >10 per genotype. (*C*) Hematoxylin and eosin (H&E) staining and quantification of growth plate parameters at age 3 weeks. Misaligned chondrocytes highlighted in box 1 (magnified in box 3). Retained chondrocytes at the chondro-osseous boundary highlighted in box 2 (magnified in box 4). Areas of hypocellularity indicated by and asterisk. RZ = resting zone; PZ = proliferative zone; HZ = hypertrophic zone. Scale bar = 100 μm. n = 3 per genotype. (*D*) IHC staining for the hypertrophic marker type X collagen at age 3 weeks (collagen X: red; nuclei counterstained with DAPI: blue) and measurement of zone of staining. Scale bar = 100 μm. n = 3 per genotype. (*E*) TUNEL and analysis of IHC staining for BrdU at age 3 weeks. BV/TV = bone volume/total volume; Tb.N = trabecular number; RZ = resting zone; PZ = proliferative zone; HZ = hypertrophic zone. n = 3 per genotype. All graphs are displayed as mean ± SD, *p < 0.05, **p < 0.005.

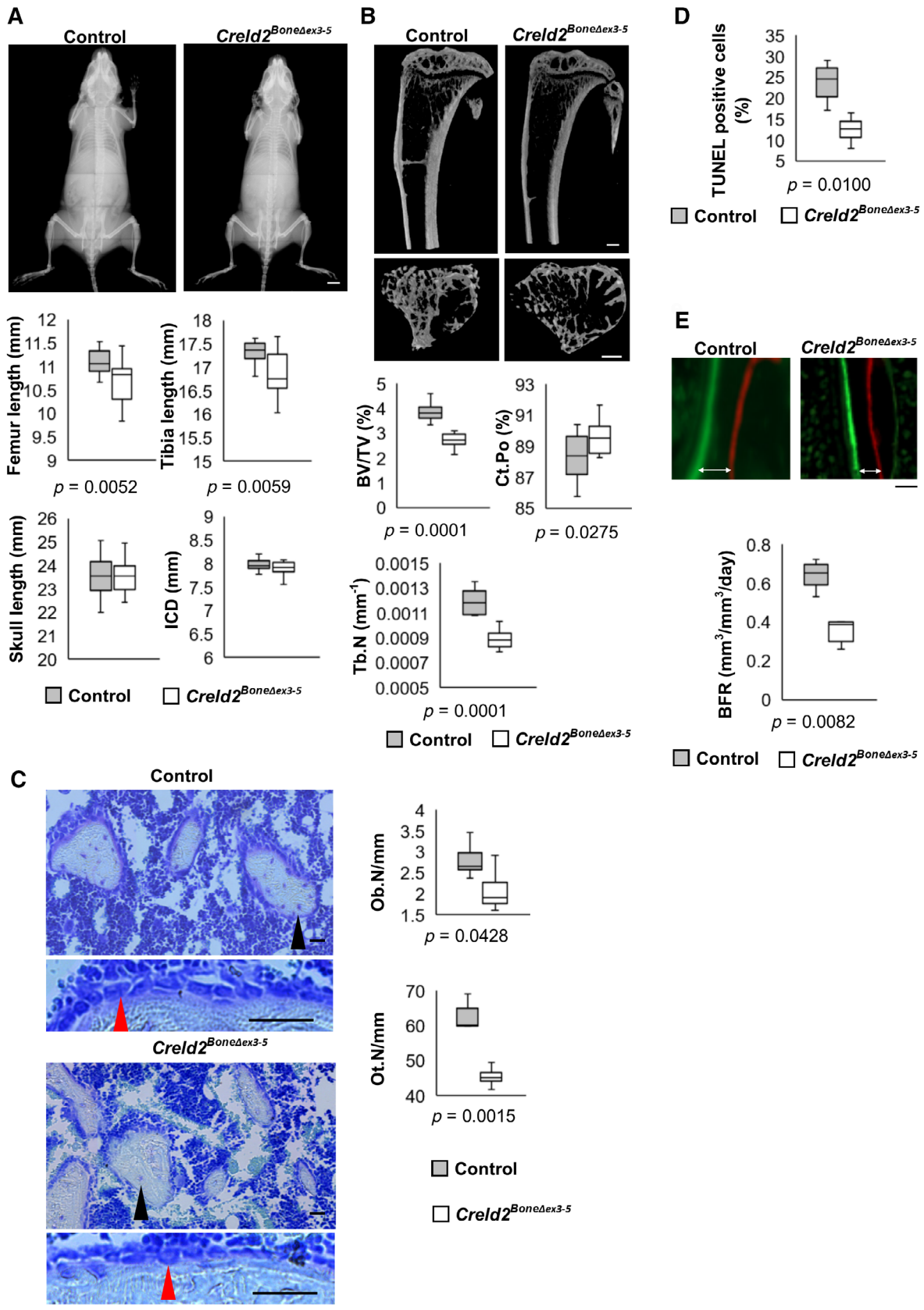

Fig. 2. *Creld2*$^{Bone\Delta Ex3-5}$ display an osteopenic phenotype due to impaired osteoblast activity. (*A*) Representative X-ray images at age 9 weeks and bone measurements. Scale bar = 5 mm. *n* = >10 per genotype. (*B*) Bone microarchitecture analysis at age 9 weeks from μCT (representative images of sagittal and transverse projection). Scale bar = 500 μm. *n* = >10 per genotype. (*C*) Toluidine blue staining and quantification of osteoblast (cuboidal osteoblasts lining the bone indicated with red arrow)/osteocyte (indicated with black arrow) numbers at age 9 weeks. Scale bar = 100 μm. *n* = 5 per genotype. (*D*) TUNEL analysis of apoptosis of osteoblasts in vitro (*n* = 3 per genotype). (*E*) Fluorochrome labeling of bone and analysis of dynamic bone parameters. BFR = bone formation rate. Scale bar = 25 μm. *n* = 8 per genotype. (*E*) TUNEL and analysis of immunohistochemical staining of BrdU (*n* = 3 per genotype). BV/TV = bone volume/total volume; Tb.N = trabecular number; Ct.Po = cortical porosity; Ob.N/BS = osteoblast number/bone surface; Ot.N/BA = osteocyte number/bone area. All graphs are displayed as mean ± SD, **p* < 0.05, ***p* < 0.005.

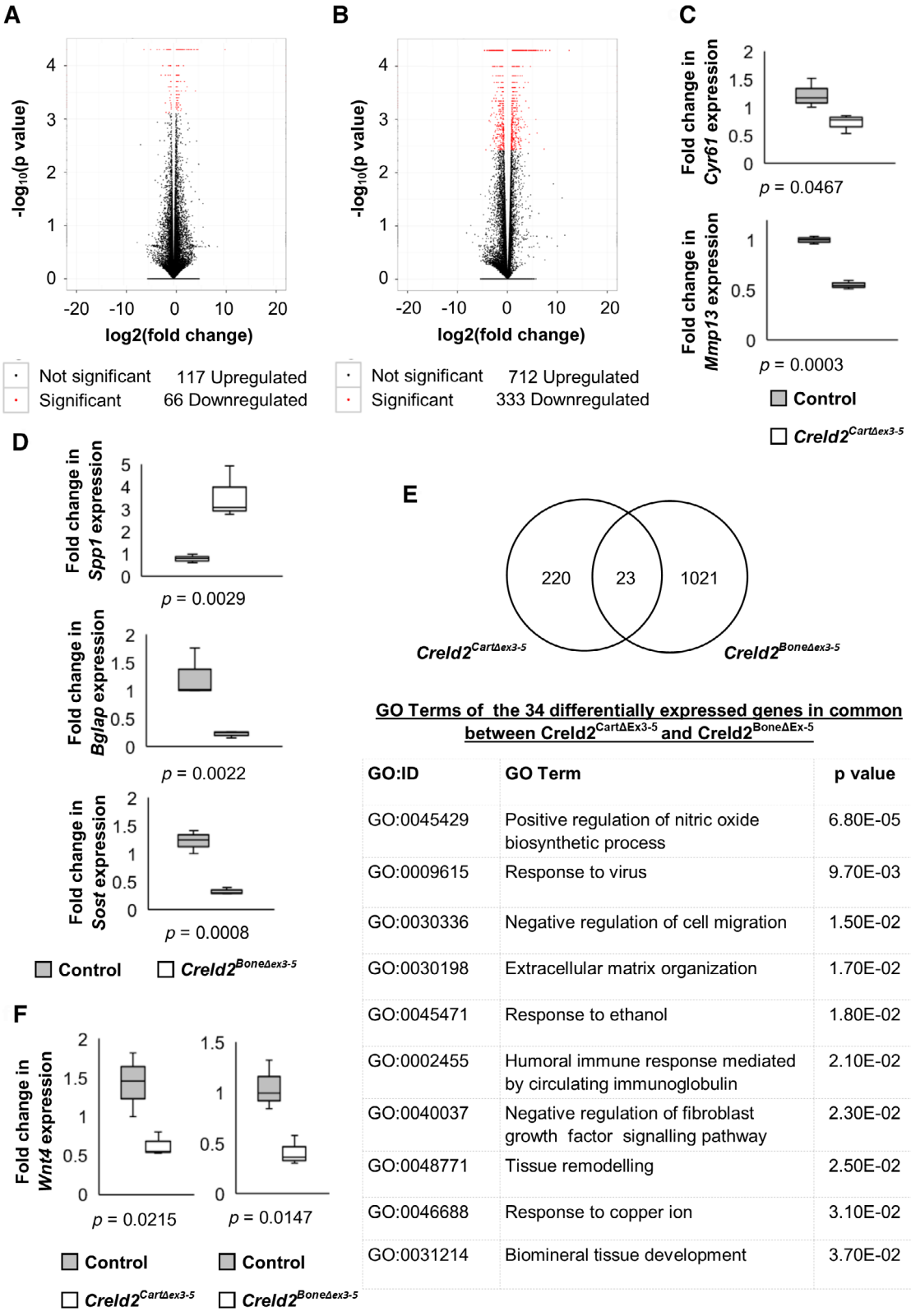

GO Terms of the 34 differentially expressed genes in common between Creld2$^{CartΔEx3-5}$ and Creld2$^{BoneΔEx-5}$

GO:ID	GO Term	p value
GO:0045429	Positive regulation of nitric oxide biosynthetic process	6.80E-05
GO:0009615	Response to virus	9.70E-03
GO:0030336	Negative regulation of cell migration	1.50E-02
GO:0030198	Extracellular matrix organization	1.70E-02
GO:0045471	Response to ethanol	1.80E-02
GO:0002455	Humoral immune response mediated by circulating immunoglobulin	2.10E-02
GO:0040037	Negative regulation of fibroblast growth factor signalling pathway	2.30E-02
GO:0048771	Tissue remodelling	2.50E-02
GO:0046688	Response to copper ion	3.10E-02
GO:0031214	Biomineral tissue development	3.70E-02

Fig. 3. RNA-sequencing indicates that the lack of *Creld2* disrupts WNT signaling in chondrocytes and osteoblasts and impairs osteogenic and chondrogenic differentiation. Volcano plots of differential gene expression in *Creld2*$^{CartΔEx3–5}$ chondrocytes (*A*) and *Creld2*$^{BoneΔEx3–5}$ mature osteoblasts (*B*). Differentially expressed genes with statistical significance (false discovery rate [FDR] adjusted *p* value <0.05) are indicated with a red dot (fold change >1.5-fold) and nonsignificant genes are indicated with a black dot. (*C*) qRT-PCR analysis of *Cyr61* and *Mmp13* in *Creld2*$^{CartΔEx3–5}$ and control chondrocytes. (*D*) qRT-PCR analysis of *Spp1*, *Bglap*, and *Sost* in *Creld2*$^{BoneΔEx3–5}$ and control mature osteoblasts. (*E*) Venn diagram of differential genes (FDR adjusted *p* value <0.05) between *Creld2*$^{CartΔEx3–5}$ chondrocytes and *Creld2*$^{BoneΔEx3–5}$ mature osteoblasts. Table of GO terms for the 23 differentially expressed genes in common between *Creld2*$^{CartΔEx3–5}$ chondrocytes and *Creld2*$^{BoneΔEx3–5}$ mature osteoblasts (FDR adjusted *p* value <0.05). (*F*) qRT-PCR analysis of *Wnt4* expression in *Creld2*$^{CartΔEx3–5}$ and control chondrocytes and *Creld2*$^{BoneΔEx3–5}$ and control mature osteoblasts. $n = 3$ per genotype. Graphs are displayed as mean ± SD, $^{*}p < 0.05$, $^{**}p < 0.005$.

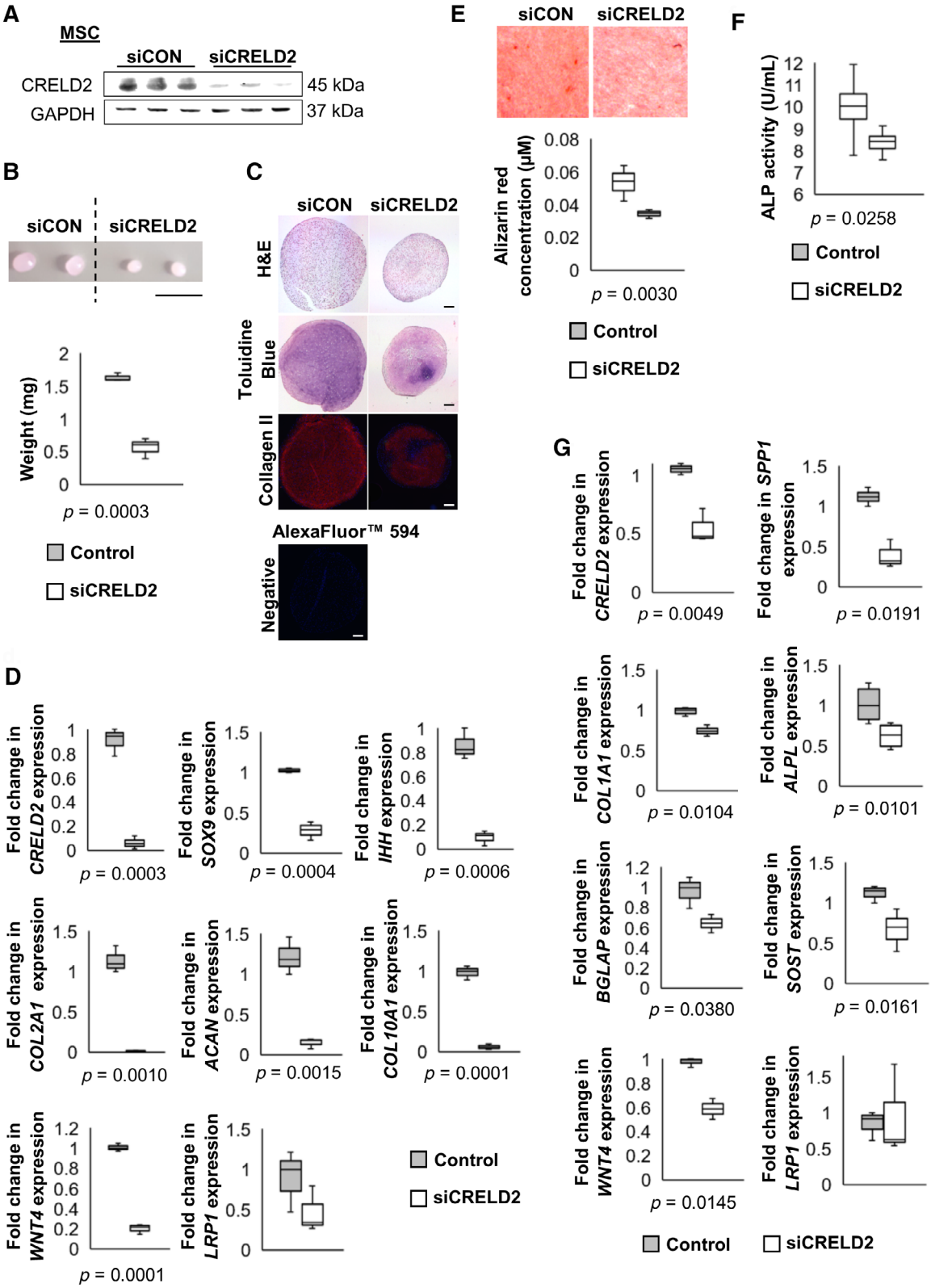

Fig. 4. CRELD2 plays a role in chondrogenic and osteogenic differentiation of hMSCs. (*A*) Western blot showing successful knockdown of *CRELD2* expression using gene silencing siRNA. Equal loading shown by GAPDH. (*B*) Weights of control (siCON) and *CRELD2* knockdown (siCRELD2) chondrocyte pellets. Scale bar = 5 mm. (*C*) Histology staining of chondrocyte pellets (H&E, toluidine blue staining) showing proteoglycans and immunohistochemistry for collagen II expression (collagen II: red; nuclei counterstained with DAPI: blue). Scale bar = 200 μm. (*D*) qRT-PCR analysis of *CRELD2* and chondrocyte marker genes in siCON and siCRELD2 chondrocytes. (*E*) Alizarin red staining of matrix mineralization in the monolayer culture of hMSC-derived osteoblasts and optical density quantification of staining intensity. $n = 3$ per genotype. (*F*) Quantification of alkaline phosphatase (ALP) activity in siCON and siCRELD2 osteoblasts. (*G*) qRT-PCR analysis of *CRELD2* and osteoblast marker genes in siCON and siCRELD2 osteoblasts. $n = 3$ per genotype. Graphs are displayed as mean ± SD, $^{*}p < 0.05$, $^{**}p < 0.005$.

involved in the cell cycle, apoptosis, and ossification. qPCR was used to verify the expression of four key genes differentially expressed in *Creld2* knockout osteoblasts (Fig. 3*D*). The expression of the immature osteoblast marker *Spp1* was upregulated, whereas *Bglap* and *Sost*, both markers of mature osteoblasts and osteocytes, were downregulated. Overall these data further confirm that the deletion of *Creld2* in chondrocytes and mature osteoblasts results in impaired differentiation and maturation.

Twenty-three genes (17 upregulated, 6 downregulated) were differentially expressed in common between $Creld2^{CartΔEx3–5}$ chondrocytes and $Creld2^{BoneΔEx3–5}$ mature osteoblasts (Supplemental Table S3). These clustered into genes involved in extracellular matrix organization, biomineral tissue development, and negative regulation of fibroblast growth factor signaling (Fig. 3*E*). Interestingly *Wnt4*, encoding a secreted signaling protein that can modulate chondrocyte maturation[34] and enhance osteogenic differentiation,[35] was downregulated in both $Creld2^{CartΔEx3–5}$ chondrocytes and $Creld2^{BoneΔEx3–5}$ mature osteoblasts (Fig. 3*F*), which could explain the delay in chondrocyte and osteoblast maturation observed in both the $Creld2^{CartΔEx3–5}$ and $Creld2^{BoneΔEx3–5}$ mice, respectively.

CRELD2 modulates WNT signaling during chondrogenic and osteogenic differentiation

We further examined the role of CRELD2 in chondrocyte and osteoblast differentiation by silencing *CRELD2* expression using siRNA during in vitro chondrogenic and osteogenic differentiation of human mesenchymal stem cells (hMSCs). Successful knockdown of CRELD2 was confirmed by Western blotting before MSC differentiation (Fig. 4*A*). *CRELD2* knockdown (siCRELD2) resulted in smaller cartilage pellets compared with control (siCON) pellets, indicating that CRELD2 plays a prominent role in regulating early chondrogenesis (Fig. 4*B*, *C*). siCRELD2 pellets showed a disrupted ECM composition characterized by a reduction in toluidine blue (proteoglycan stain) and type II collagen staining (Fig. 4*C*). Additionally, expression levels of several chondrogenic markers (*SOX9, IHH, COL2A1, ACAN*, and *COL10A1*) were significantly reduced in siCRELD2 chondrocytes, indicating chondrocyte differentiation was impaired after the knockdown of *CRELD2* (Fig. 4*D*).

Osteogenic differentiation of siCRELD2 hMSCs was also disrupted, as characterized by a significant reduction in matrix mineralization (Fig. 4*E*) and alkaline phosphatase (ALP) activity (Fig. 4*F*). Several well-established osteoblast marker genes were differentially expressed after the knockdown of *CRELD2* (Fig. 4*G*). For example, *COL1A1* and *ALPL* involved in bone matrix formation and mineralization; *SPP1*, *BGLAP*, and *SOST*, markers of immature and mature osteoblasts and osteocytes, respectively, were significantly reduced in siCRELD2 osteoblasts, indicating the knockdown of *CRELD2* impaired osteoblast differentiation and osteogenesis.

It was of particular significance that both siCRELD2 hMSC-derived chondrocytes and osteoblasts exhibited a significant reduction in *WNT4* expression (Fig. 4*D*, *G*), consistent with its reduced expression levels in primary chondrocytes and osteoblasts from the *Creld2* knockout mice (Fig. 3). These data suggest that CRELD2 plays an important role in hMSC chondrogenic and osteogenic differentiation potentially via modulating WNT4 signaling.

CRELD2 promotes the membrane expression of LRP1

Immunocytochemistry was used to analyze the subcellular localization of CRELD2 in primary chondrocytes. CRELD2 co-localized with the ER marker heat shock protein 90 kDa beta member 1 (also known as GRP94), the Golgi marker Golgi apparatus protein 1 (GLG1), and the exosomal marker Cluster of differentiation 81 (CD81), thereby suggesting a potential role for this chaperone in trafficking proteins from the ER through the secretory pathway (Supplemental Fig. S4).

To further elucidate the role of CRELD2 in chondrocyte and osteoblast biology, putative CRELD2 binding partners were identified by co-immunoprecipitation (Co-IP) performed using recombinant V5-tagged CRELD2 overexpressed in the SW1353 (chondrocyte-like) and the SAOS2 (osteoblast-like) cell lines as previously described.[12] Co-IP proteins were identified by LC–MS/MS performed on Co-IP protein pools and 66 potential CRELD2 binding partners in SW1353 cells (top 50 shown in Supplemental Table S4) and 99 potential CRELD2 binding partners in SAOS2 cells (top 50 shown in Supplemental Table S5) were identified. Interestingly, there were only 28 binding partners in common between SW1353 and SAOS2 cells (Supplemental Table S6). In both cell types, CRELD2 was found to bind to DNAJ proteins, peptidyl prolyl-isomerases (PPIs) and PDIs that function as chaperones involved in the folding and processing of nascent proteins, further confirming its ER localization. CRELD2 also bound to protein complexes involved in the processing of collagen fibrils, such as collagen prolyl-hydroxylases as well as several collagen alpha chains including collagen alpha-2[1] suggesting a putative role for CRELD2 in collagen folding; however, there was no evidence of collagen retention in knockout cells. Furthermore, CRELD2 was also found to bind the receptor low-density lipoprotein receptor-related protein 1 (LRP1) and the mesoderm development LRP chaperone (MESD) in both cell lines, indicating that it may function as a chaperone in assisting the folding, maturation, and transport of LRP1 through the secretory pathway during skeletal development.

To study the role of CRELD2 in LRP1 membrane trafficking, *CRELD2* expression was knocked down in SW1353 and SAOS2 cells using siRNA. Successful knockdown was confirmed by qPCR and Western blotting (Fig. 5*A*, *B*). It is important to note that the expression of LRP1 was not changed at either the RNA or protein level after the ablation of *CRELD2* in siRNA-treated SW1353 and SAOS2 cells (Fig. 5*A*, *B*). However, live immunolabeling (Fig. 5*C*) and Western blotting (Fig. 5*D*) of the membrane fraction revealed that there was significantly less staining of LRP1 at the membrane in both SW1353 and SAOS2 knockdown cells. Thus, in chondrocytes and osteoblasts, CRELD2 potentially functions as a novel LRP1 chaperone through the secretory pathway and promotes LRP1 expression at the cell surface.

WNT4 expression is driven by LRP1 in chondrocytes but not in osteoblasts

To determine whether reduced LRP1 membrane expression results in impaired chondrocyte and osteoblast maturation, *LRP1* expression was silenced during in vitro chondrogenic and osteogenic differentiation of hMSCs using siRNA. Successful knockdown of LRP1 was confirmed by Western blotting (Fig. 6*A*).

The knockdown of *LRP1* during chondrogenesis resulted in significantly smaller siLRP1 cartilage pellets (Fig. 6*B*, *C*); however, this difference in size was not as pronounced as observed with siCRELD2 cartilage pellets. siLRP1 pellets displayed reduced matrix staining for type II collagen; however, unlike the altered proteoglycan composition observed in siCRELD2 pellets, matrix staining (Fig. 6*C*) and gene expression levels (Fig. 6*D*) for the major cartilage proteoglycan aggrecan were comparable between control and siLRP1 pellets, suggesting that CRELD2

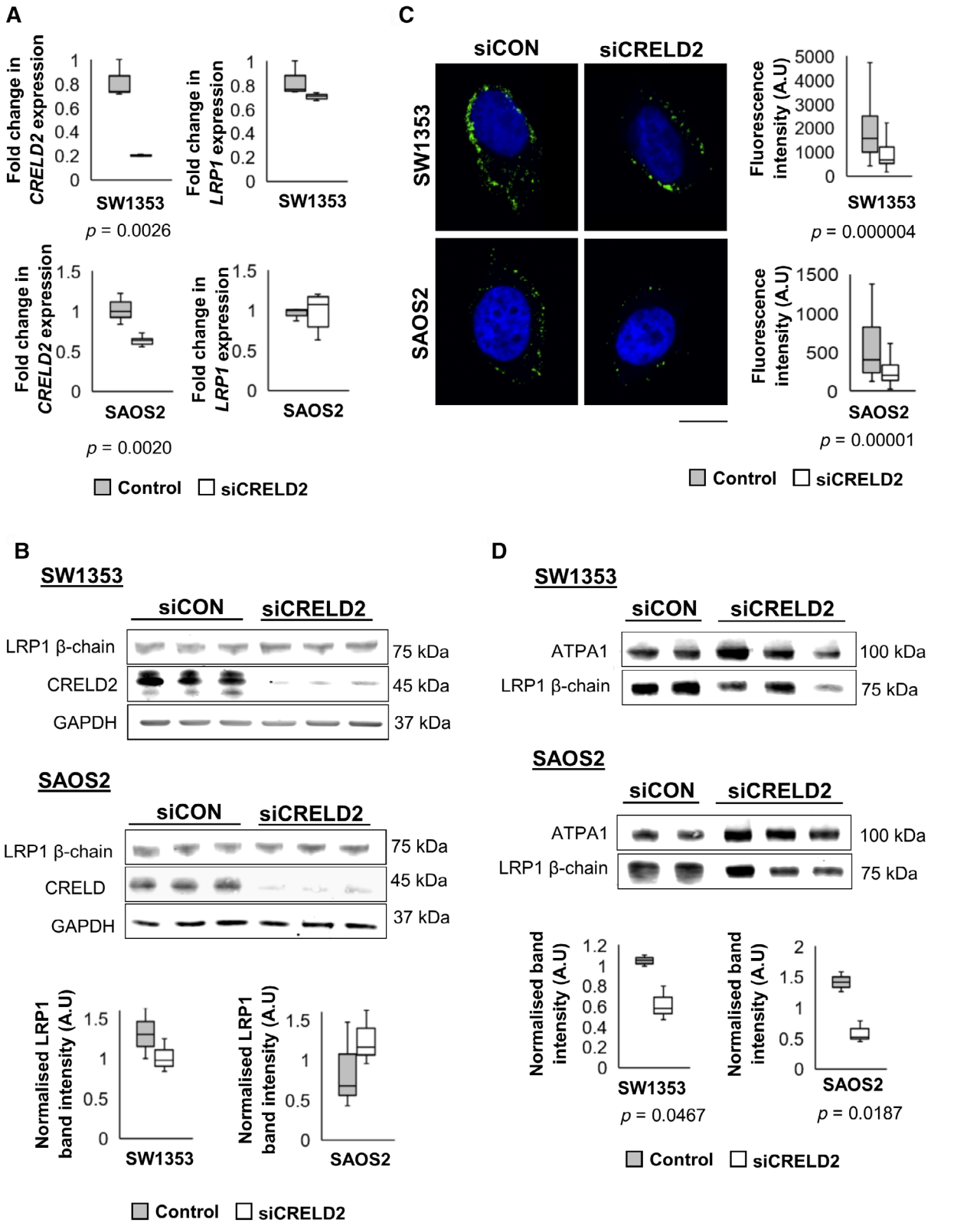

Fig. 5. CRELD2 promotes the membrane expression of LRP1. (*A*) qRT-PCR analysis of *CRELD2* and *LRP1* in siCON and siCRELD2 SW1353 chondrocyte-like and SAOS2 osteoblast-like cells. (*B*) Western blot showing successful knockdown of *CRELD2* expression using gene silencing siRNA in SW1353 and SAOS2 cells. The levels of LRP1 in control and knockdown cells were determined by Western blot band densitometry. Equal loading shown by GAPDH. (*C*) Representative images of live cell surface LRP1 labelling and quantification of immunocytochemical staining of membrane LRP1 in control and knockdown cells. (*D*) Western blot showing LRP1 expression in the membrane fraction from control and knockdown cells. These levels were quantified by band densitometry. Equal loading shown by Alpha-1 sodium potassium ATPase (plasma membrane marker). Scale bar = 10 μm. $n = 3$ per genotype. Graphs are displayed as mean ± SD, $^{*}p < 0.05$, $^{**}p < 0.005$.

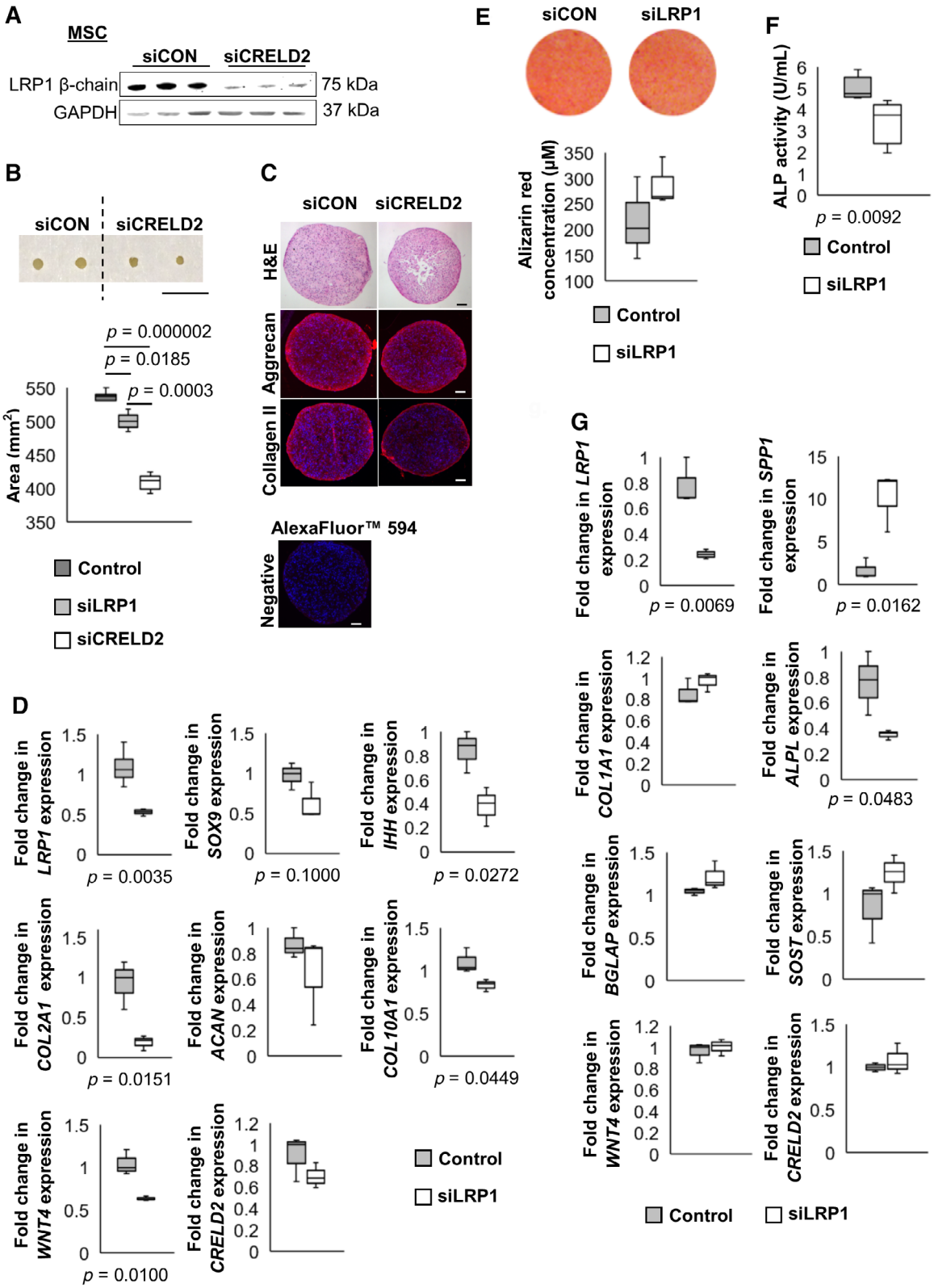

Fig. 6. LRP1 promotes WNT4 expression during chondrogenic differentiation of MSCs but not during osteogenesis. (*A*) Western blot showing successful knockdown of *LRP1* expression using gene silencing siRNA. Equal loading shown by GAPDH. (*B*) Representative images and quantification of the average area of control (siCON) and *LRP1* knockdown (siLRP1) chondrocyte mini pellets compared with the average area of *CRELD2* knockdown (siCRELD2) mini pellets. Scale bar = 100 μm. (*C*) Histology staining of chondrocyte pellets (H&E and immunohistochemistry for collagen II and Aggrecan expression). Scale bar = 100 μm. (*D*) qRT-PCR analysis of *LRP1* and chondrocyte marker genes in siCON and siLRP1 chondrocytes. (*E*) Alizarin red staining of matrix monolayer of MSC-derived osteoblasts and quantification of staining intensity. (*F*) Quantification of ALP activity in siCON and siLRP1 osteoblasts. (*G*) qRT-PCR analysis of *LRP1* and osteoblast marker genes in siCON and siLRP1 osteoblasts. $n = 3$ per genotype. Graphs are displayed as mean ± SD, $^{*}p < 0.05$, $^{**}p < 0.005$.

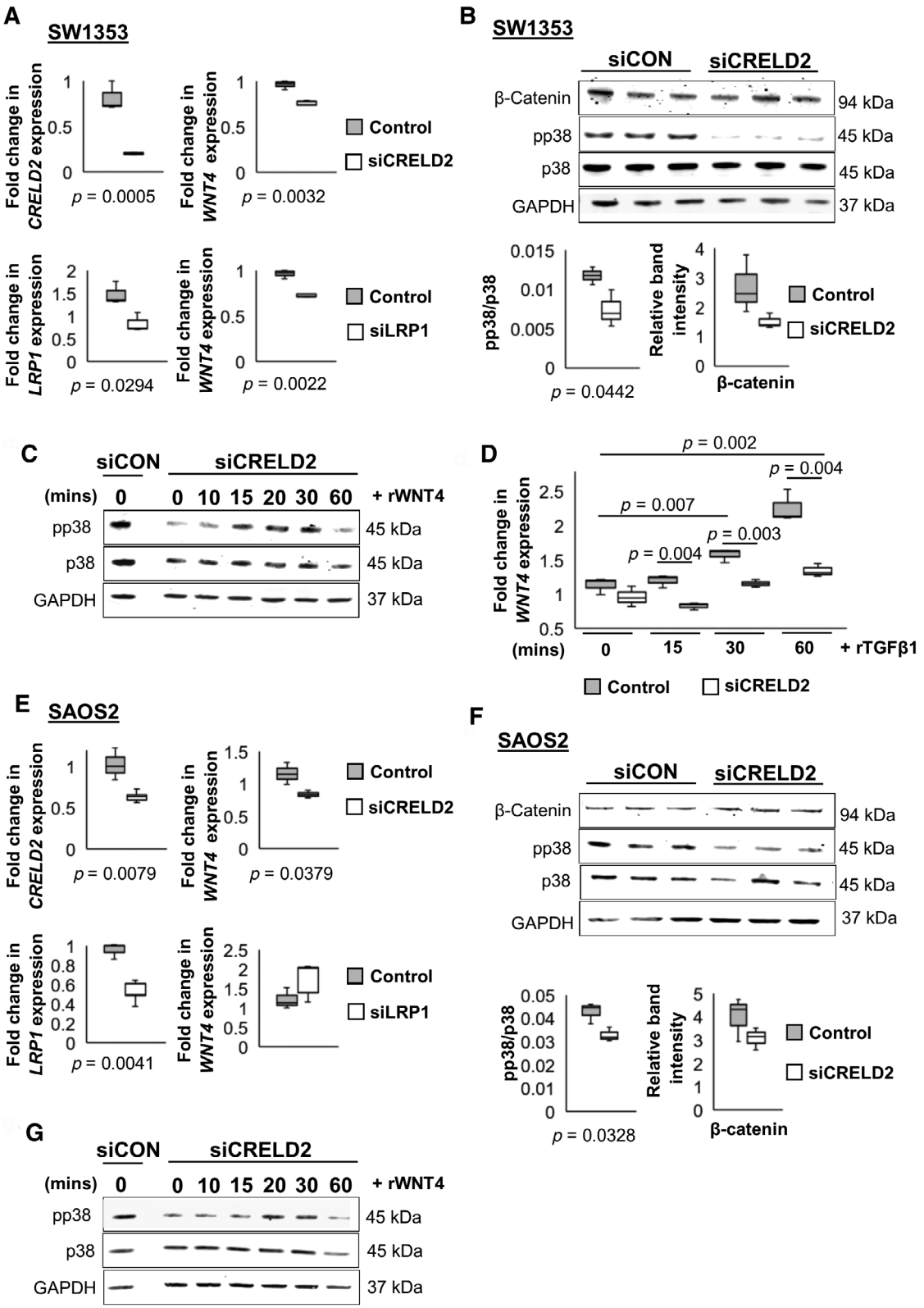

Fig. 7. The lack of CRELD2 in chondrocytes and osteoblasts disrupts p38 MAPK signaling. (*A*) qRT-PCR analysis of *CRELD2, LRP1*, and *WNT4* in control (siCON) and CRELD2 (siCRELD2) and LRP1 (siLRP1) knockdown SW1353 cells. (*B*) Western blot showing β-catenin, p38, and phospho p38 (pp38) expression in siCON and siCRELD2 SW1353 chondrocyte-like cells. Levels were determined by Western blot densitometry. (*C*) Western blot showing p38 and pp38 expression in siCON and siCRELD2 SW1353 cells after treatment with recombinant WTN4 (rWNT4). (*D*) qRT-PCR analysis of *WNT4* expression in control and siLRP1 SW1353 cells after treatment with recombinant TGF-β1 (rTGF-β1). (*E*) qRT-PCR analysis of *CRELD2, LRP1*, and *WNT4* in control and knockdown SAOS2 cells. (*F*) Western blot showing β-catenin, p38, and pp38 expression in siCON and siCRELD2 SAOS2 osteoblast-like cells. Levels were determined by Western blot densitometry. (*G*) Western blot showing p38 and pp38 expression in siCON and siCRELD2 SAOS2 cells after treatment with rWNT4. Equal loading shown by GAPDH. $n = 3$ per genotype. All graphs are displayed as mean ± SD, $^{*}p < 0.05$, $^{**}p < 0.005$.

may play additional roles during chondrogenesis besides chaperoning LRP1. The expression levels of several chondrogenic markers (*IHH*, *COL2A1*, and *COL10A1*) were significantly reduced in siLRP1 chondrocytes, confirming that chondrogenesis was disrupted after the knockdown of *LRP1* expression (Fig. 6*D*).

Unlike the knockdown of *CRELD2*, the knockdown of *LRP1* did not affect matrix mineralization (Fig. 6*E*) despite a significant decrease in ALP activity in siLRP1 osteoblasts (Fig. 6*F*). Many of the osteoblast markers were also unaffected after the knockdown of *LRP1* (Fig. 6*G*); however, *ALPL*, involved in matrix mineralization, was downregulated and the expression of the immature osteoblast

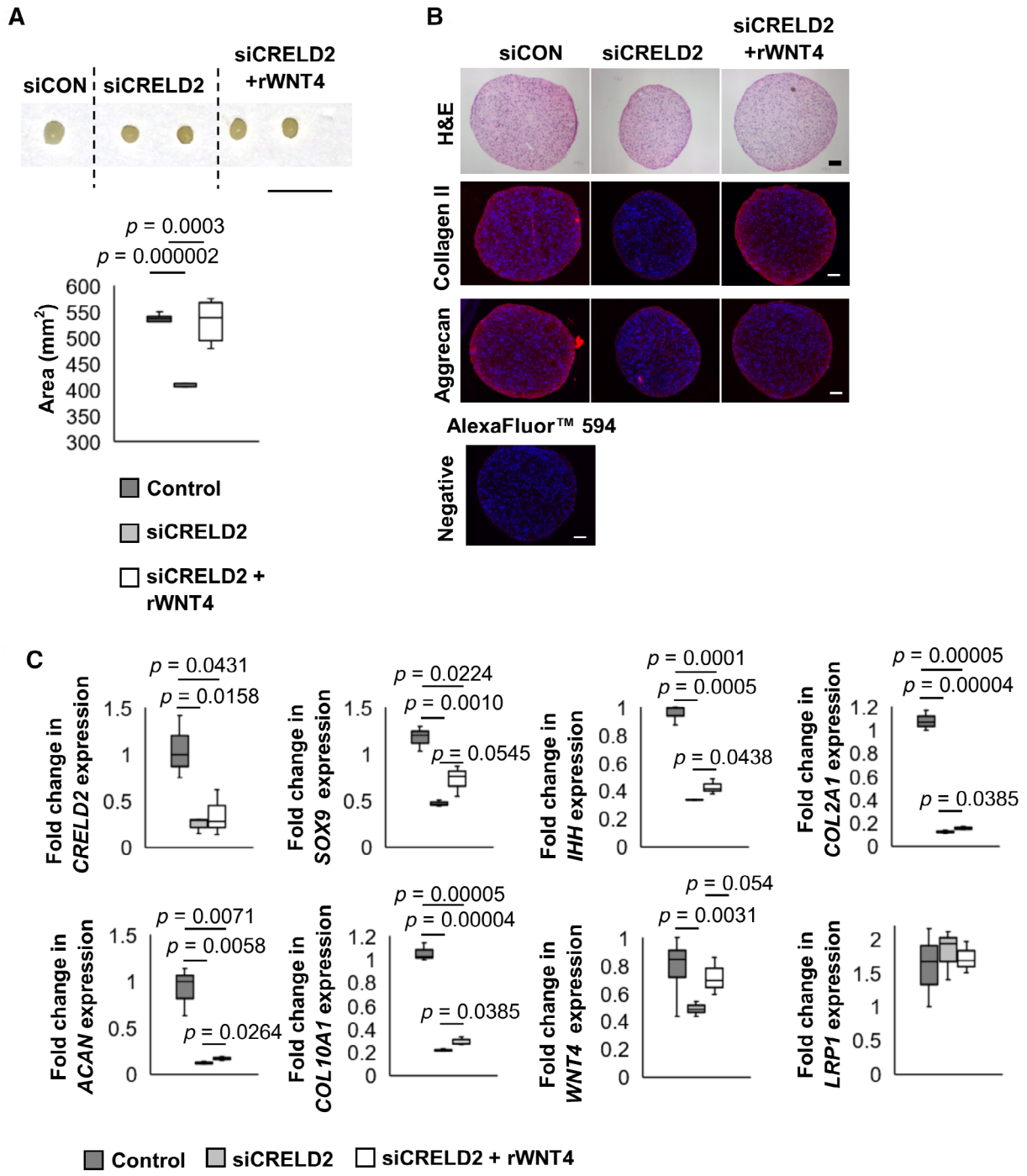

Fig. 8. Exogenous WNT4 treatment restores chondrogenic differentiation after the knockdown of CRELD2. (*A*) Representative images and quantification of the average area of control (siCON) and *CRELD2* knockdown (siCRELD2) mini chondrocyte pellets with and without recombinant WNT4 (rWNT4) treatment. Scale bar = 100 µm. (*B*) Histology staining of chondrocyte pellets (H&E and immunohistochemistry for collagen II and Aggrecan in red; DAPI nuclear counterstain in blue). Scale bar = 100 µm. (*C*) qRT-PCR analysis of *CRELD2* and chondrocyte marker genes in siCON and siCRELD2 +/-rWNT4 chondrocytes. $n = 3$ per genotype. All graphs are displayed as mean ± SD, $^{*}p < 0.05$, $^{**}p < 0.005$.

marker *SPP1* was upregulated in siLRP1 osteoblasts, indicating that LRP1 potentially plays a role in early osteoblast differentiation.

WNT4 expression was significantly reduced in siLRP1 chondrocytes (Fig. 6*D*) but was unchanged in siLRP1 osteoblasts (Fig. 6*G*). These data suggest that LRP1 drives *WNT4* expression during chondrogenic differentiation, but the expression of *WNT4* is LRP1-independent during osteogenesis.

WNT4 signals via p38 mitogen-activated protein kinase (MAPK) in chondrocytes and osteoblasts

As previously shown in primary chondrocytes and during hMSC differentiation, the knockdown of *CRELD2* in the chondrocyte-like SW1353 cell line resulted in a significant reduction of *WNT4* expression (Fig. 7*A*). As observed in siLRP1 chondrocytes, *WNT4*

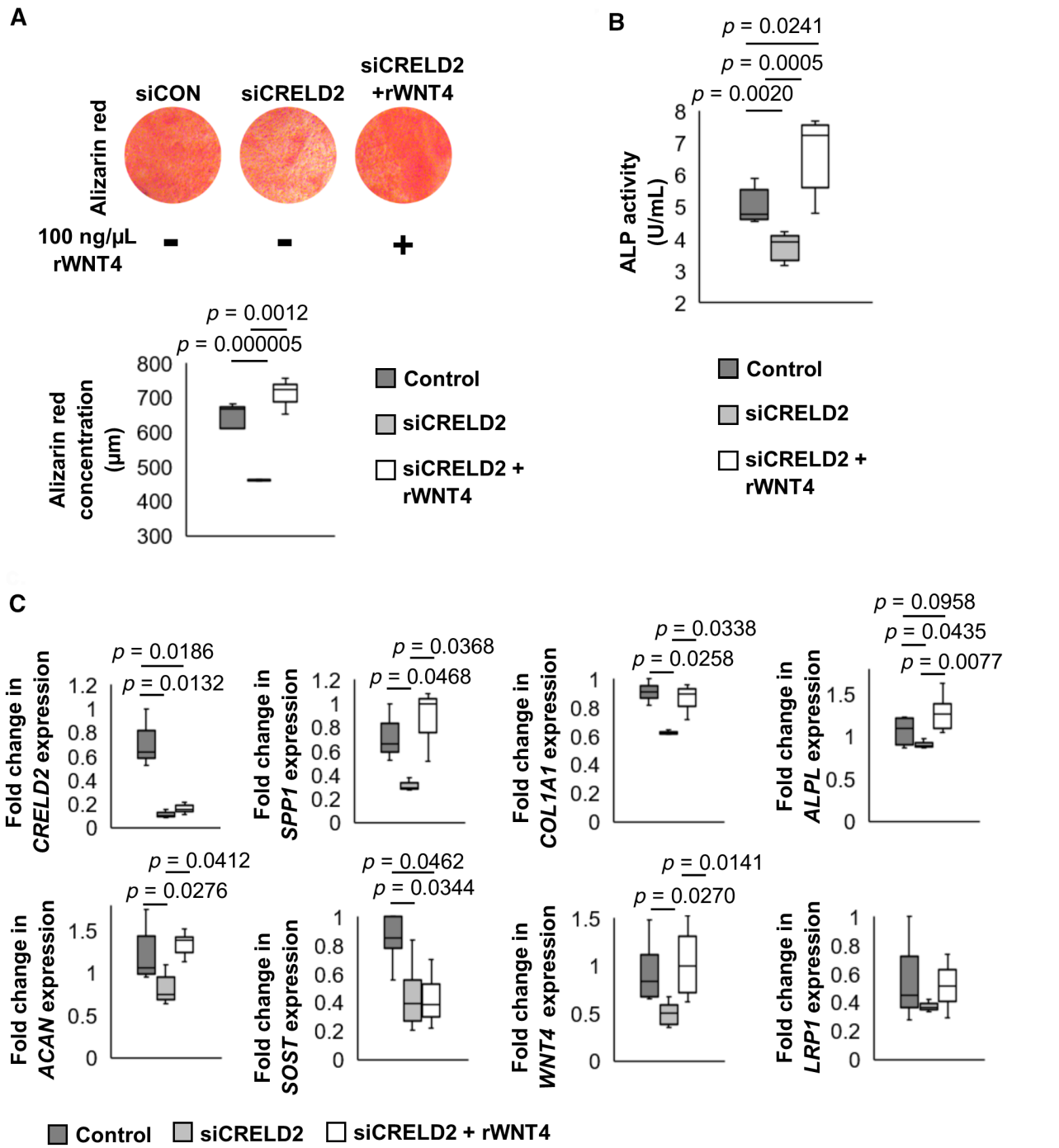

Fig. 9. Exogenous WNT4 treatment restores osteogenic differentiation after the knockdown of CRELD2. (*A*) Alizarin red staining of matrix monolayer of MSC-derived osteoblasts and quantification of staining intensity. (*B*) Quantification of ALP activity in siCON and siCRELD2 +/-rWNT4 osteoblasts. (*C*) qRT-PCR analysis of *CRELD2* and osteoblast marker genes in siCON and siCRELD2 +/-rWNT4 osteoblasts. $n = 3$ per genotype. All graphs are displayed as mean ± SD, $*p < 0.05$, $**p < 0.005$.

expression was also reduced in siLRP1 SW1353 cells, providing further evidence that LRP1 drives WNT4 expression in chondrocytes (Fig. 7*A*).

Previous studies have shown that p38 MAPK regulates noncanonical WNT signaling.[35,36] Pharmacological inhibition of p38 signaling inhibits chondrogenesis, suggesting an obligatory role for p38 MAPK signaling in chondrocyte differentiation.[37,38] To further dissect the role of noncanonical WNT4 signaling during chondrogenesis, the p38 MAPK signaling cascade was analyzed in SW1353 cells by Western blotting. The knockdown of *CRELD2* in SW1353 cells did not affect canonical WNT signaling as β-catenin levels were unchanged; however, it significantly impaired p38 MAPK signaling as shown by a significant reduction in the pp38/p38 ratio in *CRELD2* knockdown cells (Fig. 7*B*). Moreover, the addition of recombinant WNT4 to knockdown cells restored p38 signaling 15 to 30 minutes post-treatment (Fig. 7*C*). Recent studies have shown that LRP1 modulates *WNT5A* expression in mouse embryonic fibroblasts by binding TGF-β1.[39] The expression of *WNT4* in SW1353 cells was upregulated after TGF-β1 treatment, whereas in *LRP1* knockdown SW1353 cells, *WNT4* expression was significantly reduced with and without TGF-β1 treatment (Fig. 7*D*), indicating that LRP1 modulates WNT4 expression via TGF-β1 in chondrocytes.

As previously observed in primary osteoblasts and hMSCs, the knockdown of *CRELD2* in the osteoblast-like SAOS2 cell line also resulted in reduced expression of *WNT4* (Fig. 7*E*). The levels of *WNT4* expression were significantly higher in siLRP1 SAOS2 cells (Fig. 7*E*), opposite to that observed in siLRP1 SW1353 cells. These data highlight that WNT4 expression is regulated differently in chondrocytes and osteoblasts and that *WNT4* downregulation in siCRELD2 osteoblasts is likely to be independent of LRP1. Studies have shown that noncanonical p38 MAPK signaling is crucial for osteogenesis as p38 inhibitors blocked osteogenic differentiation.[40,41] Western blotting was therefore used to analyze p38 MAPK signaling in siCRELD2 SASO2 cells. As demonstrated in the SW1353 cells, canonical WNT/β-catenin signaling in SAOS2 cells was unaffected after the knockdown of *CRELD2*; however, p38 MAPK signaling was impaired since there was a significant reduction in the pp38/p38 ratio in knockdown cells (Fig. 7*F*). As already demonstrated in SW1353 cells, this reduction in p38 signaling was restored by the addition of recombinant WNT4 to siCRELD2 SAOS2 cells (Fig. 7*G*). Thus, CRELD2 is important for WNT4 signaling via noncanonical p38 MAPK that has previously been shown to promote chondrogenic and osteogenic differentiation.

Exogenous WNT4 rescues the impaired chondrogenic and osteogenic differentiation of knockdown *CRELD2* hMSCs

Because WNT4 promotes chondrocyte[3] and osteoblast differentiation[4] we next wished to determine the effects of exogenous WNT4 on in vitro chondrogenic and osteogenic differentiation of *CRELD2* knockdown hMSCs.

Consistent with experiments shown in Fig. 4, chondrogenesis was disrupted after *CRELD2* knockdown because siCRELD2 pellets were significantly smaller (Fig. 8*A, B*) and had a disrupted ECM composition with reduced staining for type II collagen and aggrecan (Fig. 8*B*). The addition of exogenous WNT4 rescued this abnormal cell phenotype; indeed siCRELD2 pellets treated with WNT4 were significantly larger than the siCRELD2 pellets and were an equivalent size to control pellets (Fig. 8*A*). The expression of ECM structural proteins was restored in siCRELD2 pellets treated with WNT4 (Fig. 8*B*) and in addition the expression levels of several chondrogenic markers, which were significantly reduced in siCRELD2 chondrocytes, were significantly increased after the addition of WNT4 (Fig. 8*C*).

We have demonstrated that the in vitro osteogenic differentiation of hMSCs was delayed after *CRELD2* knockdown (Fig. 4*E-G*). For example, matrix mineralization and ALP activity were significantly reduced in siCRELD2 osteoblasts and this was also rescued by the addition of exogenous WNT4 (Fig. 9*A, B*). Moreover, the knockdown of *CRELD2* resulted in downregulation of several osteoblast marker genes; however, their expression returned to control levels in siCRELD2 osteoblasts treated with WNT4 (except for the osteocyte marker gene *SOST*) (Fig. 9*C*).

These data indicate that the addition of WNT4 restores the chondrogenic and osteogenic differentiation of *CRELD2* knockdown hMSCs and confirms that CRELD2 plays an important role in chondrocyte differentiation and osteoblast maturation by directly modulating WNT4 signaling.

Discussion

CRELD2 has been identified as an ER-stress-inducible gene expressed in several tissues[16,17]; however, very little is known about its role in skeletal development and homeostasis. Here we describe the first in-depth study of *Creld2* transgenic mice and identify a novel important role for CRELD2 in regulating chondrogenic and osteogenic differentiation.

Creld2$^{CartΔEx3-5}$ mice displayed a chondrodysplasia-like phenotype with abnormal cartilage growth plates, whereas *Creld2*$^{BoneΔEx3-5}$ mice had an osteopenic phenotype with low bone density and altered trabecular architecture. Transcriptomic analysis of the knockout tissues showed dysregulation of genes important for chondrocyte differentiation and proliferation and for osteoblast maturation. Moreover, in vitro chondrogenesis and osteogenesis of hMSCs was impaired after *CRELD2* knockdown, indicating that deletion of *Creld2* impairs chondrocyte and osteoblast differentiation and maturation.

WNT signaling plays a major role in controlling skeletal development and homeostasis, and, importantly, noncanonical p38 MAPK WNT signaling promotes skeletal cell differentiation[37,38,40,41] Interestingly, *Wnt4*, encoding a secreted noncanonical (β-catenin independent) WNT signaling protein that modulates chondrocyte maturation[34] and promotes osteogenic differentiation,[35] was downregulated in both cell types after the knockout of *Creld2*. We confirmed that knocking down *CRELD2* expression reduces noncanonical p38 signaling in both chondrocyte-like (SW1353) and osteoblast-like (SAOS2) cells, and importantly, this reduction is restored upon the addition of exogenous WNT4. Furthermore, we showed that the addition of recombinant WNT4 was able to rescue the delayed chondrogenic and osteogenic differentiation of siCRELD2 hMSCs.

To understand how CRELD2 regulates *WNT4* expression, putative CRELD2 binding partners were identified by co-immunoprecipitation. CRELD2 contains an imperfect KDEL ER-retention sequence (REDL[11]) that is believed to play a role in ER retrieval and is implicated in toxin endocytosis.[42] We therefore postulate that the REDL motif functions to retrieve extracellular CRELD2 back into the ER. A search of the UniProt database for proteins identified only four other mammalian proteins with an REDL motif. Two of these proteins, Canopy 4 (CPNY4) and Mesoderm development candidate 2 (MESDC2), function as chaperones and enhance the folding, maturation, and cell surface expression of receptors such as toll-like receptors[43] and low-density

lipoprotein receptors (LRP)[44–46] respectively. Additionally, studies have shown that an isoform of CRELD1, an ortholog of CRELD2, enhances the maturation and cell surface expression of acetylcholine receptors.[47] It is particularly noteworthy therefore that we have shown CRELD2 co-immunoprecipitates with LRP1, and *CRELD2* knockdown cells display less LRP1 on the plasma membrane. We therefore suggest that CRELD2 functions as a novel LRP1 chaperone by promoting the expression of LRP1 on the cell surface.

Previous studies have shown that LRP1 represses hypertrophy, and *LRP1* knockdown in mature chondrocytes results in an upregulation of the hypertrophic marker *COL10A1*.[48] Here we show for the first time that *LRP1* knockdown in hMSCs disrupted chondrogenesis and a reduction in *WNT4* expression, indicating that *WNT4* expression lies downstream of LRP1 during chondrogenesis. Additionally, we show that LRP1 modulates *WNT4* expression in chondrocytes by binding TGFβ-1. The defect caused by *LRP1* knockdown during chondrogenesis was less severe than that resulting from *CRELD2* knockdown as the reduction in chondrocyte pellet size was not as pronounced in siLRP1 pellets compared with siCRELD2 pellets, suggesting that CRELD2 may modulate chondrogenesis through other pathways. Additionally, CRELD2 also co-immunoprecipitated with the pro-chondrogenic proteins CYR61[33] and TGFβ-1[49] suggesting it may regulate a wide range of signaling processes during chondrogenesis. The knockdown of *LRP1* did not affect osteogenesis, which is consistent with previous studies showing that osteoblast differentiation was unaffected in *Lrp1* knockout mice. However, the mice displayed an osteoporotic phenotype due to increased osteoclastogenesis[50] further supporting the contention that LRP1 limits receptor activation of RANKL and osteoclastogenesis.[51] We found reduced membrane expression of LRP1 in si*CRELD2* SAOS2 cells and showed that RANKL is upregulated after *Creld2* knockout in osteoblasts. This suggests that CRELD2 chaperoning of LRP1 to the cell membrane acts as a mediator of the RANKL/OPG signaling axis and therefore of osteoblast–osteoclast cross-talk. Moreover, *WNT4* expression was not reduced in si*LRP1* osteoblasts, suggesting that CRELD2 modulates osteoblast WNT4 expression and maturation via a different pathway, potentially through directly binding to TGFβ-1 and stimulating *WNT4* expression.[52]

To summarize, our results propose a novel and important role of CRELD2 in chondrogenesis and osteogenesis, identifying it as a novel modulator of WNT signaling and as an evolutionarily conserved chaperone of LRP1, promoting its expression at the cell surface (Supplemental Fig. S5). To date, no human disease causing mutations has been identified in *CRELD2*, but due to its role in skeletogenesis, it is intriguing to speculate that it might be a potential genetic locus for skeletal diseases such as osteogenesis imperfecta (brittle bone disease).

Disclosures

All authors declare that they have no conflict of interest.

Acknowledgments

We thank Dr David Knight and the Biological Mass Spectrometry Facility at the University of Manchester, GATC Biotech GmbH, and the Electron Microscopy Research Services at Newcastle University for their help with sample processing and data analysis. We also acknowledge the Newcastle University Comparative Biology Centre for their help with animal husbandry during the project.

This work was funded by grants from the Wellcome Trust (grant no. 084353/Z/07/) and EU (SYBIL—European Community's Seventh Framework Programme [FP7/2007–2013] under grant agreement no. 602300).

Authors' roles: SME and CLH generated the mouse strains. EPD, RMJ, and DT conducted the experiments. EPD designed the experiments and wrote the manuscript. MC provided expertise. DAY, RB-H, and AT provided expertise and contributed to the manuscript. KAP and MDB provided expertise and resources, supervised the project, and contributed to the manuscript.

References

1. Boot-Handford RP, Briggs MD. The unfolded protein response and its relevance to connective tissue diseases. Cell Tissue Res. 2010;339(1):197–211.
2. Ma Y, Brewer JW, Diehl JA, Hendershot LM. Two distinct stress signaling pathways converge upon the CHOP promoter during the mammalian unfolded protein response. J Mol Biol. 2002;318(5):1351–65.
3. Szegezdi E, Logue SE, Gorman AM, Samali A. Mediators of endoplasmic reticulum stress-induced apoptosis. EMBO Rep. 2006;7(9):880–5.
4. Wang W, Lian N, Li L, et al. Atf4 regulates chondrocyte proliferation and differentiation during endochondral ossification by activating Ihh transcription. Development. 2009;136(24):4143–53.
5. Wei J, Sheng X, Feng D, McGrath B, Cavener DR. PERK is essential for neonatal skeletal development to regulate osteoblast proliferation and differentiation. J Cell Physiol. 2008;217(3):693–707.
6. Rupp PA, Fouad GT, Egelston CA, et al. Identification, genomic organization and mRNA expression of CRELD1, the founding member of a unique family of matricellular proteins. Gene. 2002;293(1–2):47–57.
7. Oh-hashi K, Koga H, Ikeda S, Shimada K, Hirata Y, Kiuchi K. CRELD2 is a novel endoplasmic reticulum stress-inducible gene. Biochem Biophys Res Commun. 2009;387(3):504–10.
8. Maslen CL, Babcock D, Redig JK, Kapeli K, Akkari YM, Olson SB. CRELD2: gene mapping, alternate splicing, and comparative genomic identification of the promoter region. Gene. 2006;382:111–20.
9. Robinson SW, Morris CD, Goldmuntz E, et al. Missense mutations in CRELD1 are associated with cardiac atrioventricular septal defects. Am J Hum Genet. 2003;72(4):1047–52.
10. Ortiz JA, Castillo M, del Toro ED, et al. The cysteine-rich with EGF-like domains 2 (CRELD2) protein interacts with the large cytoplasmic domain of human neuronal nicotinic acetylcholine receptor alpha4 and beta2 subunits. J Neurochem. 2005;95(6):1585–96.
11. Oh-hashi K, Kunieda R, Hirata Y, Kiuchi K. Biosynthesis and secretion of mouse cysteine-rich with EGF-like domains 2. FEBS Lett. 2011;585(15):2481–7.
12. Hartley CL, Edwards S, Mullan L, et al. Armet/Manf and Creld2 are components of a specialized ER stress response provoked by inappropriate formation of disulphide bonds: implications for genetic skeletal diseases. Hum Mol Genet. 2013;22(25):5262–75.
13. Oh-hashi K, Norisada J, Hirata Y, Kiuchi K. Characterization of the role of MANF in regulating the secretion of CRELD2. Biol Pharm Bull. 2015;38(5):722–31.
14. Kim Y, Park SJ, Manson SR, et al. Elevated urinary CRELD2 is associated with endoplasmic reticulum stress-mediated kidney disease. JCI Insight. 2017;2(23).
15. Siegert AM, Garcia Diaz-Barriga G, Esteve-Codina A, et al. A FBN1 3'UTR mutation variant is associated with endoplasmic reticulum stress in aortic aneurysm in Marfan syndrome. Biochim Biophys Acta Mol Basis Dis. 2019;1865(1):107–14.
16. Nundlall S, Rajpar MH, Bell PA, et al. An unfolded protein response is the initial cellular response to the expression of mutant matrilin-3 in a mouse model of multiple epiphyseal dysplasia. Cell Stress Chaperones. 2010;15(6):835–49.
17. Cameron TL, Bell KM, Tatarczuch L, et al. Transcriptional profiling of chondrodysplasia growth plate cartilage reveals adaptive ER-stress

networks that allow survival but disrupt hypertrophy. PLoS One. 2011;6(9):e24600.

18. Zhang J, Weng Y, Liu X, et al. Endoplasmic reticulum (ER) stress inducible factor cysteine-rich with EGF-like domains 2 (Creld2) is an important mediator of BMP9-regulated osteogenic differentiation of mesenchymal stem cells. PLoS One. 2013;8(9):e73086.
19. Schindelin J, Arganda-Carreras I, Frise E, et al. Fiji: an open-source platform for biological-image analysis. Nat Methods. 2012;9(7):676–82.
20. Bouxsein ML, Boyd SK, Christiansen BA, Guldberg RE, Jepsen KJ, Muller R. Guidelines for assessment of bone microstructure in rodents using micro-computed tomography. J Bone Miner Res. 2010;25(7):1468–86.
21. Bell PA, Dennis EP, Hartley CL, et al. Mesencephalic astrocyte-derived neurotropic factor is an important factor in chondrocyte ER homeostasis. Cell Stress Chaperones. 2019;24(1):159–73.
22. Stahelin BJ, Marti U, Solioz M, Zimmermann H, Reichen J. False positive staining in the TUNEL assay to detect apoptosis in liver and intestine is caused by endogenous nucleases and inhibited by diethyl pyrocarbonate. Mol Pathol. 1998;51(4):204–8.
23. Dempster DW, Compston JE, Drezner MK, et al. Standardized nomenclature, symbols, and units for bone histomorphometry: a 2012 update of the report of the ASBMR Histomorphometry Nomenclature Committee. J Bone Miner Res. 2013;28(1):2–17.
24. Barter MJ, Tselepi M, Gomez R, et al. Genome-wide microRNA and gene analysis of mesenchymal stem cell chondrogenesis identifies an essential role and multiple targets for miR-140-5p. Stem Cells. 2015;33(11):3266–80.
25. Barter MJ, Gomez R, Hyatt S, et al. The long non-coding RNA ROCR contributes to SOX9 expression and chondrogenic differentiation of human mesenchymal stem cells. Development. 2017;144(24):4510–21.
26. Marzia M, Sims NA, Voit S, et al. Decreased c-Src expression enhances osteoblast differentiation and bone formation. J Cell Biol. 2000;151(2):311–20.
27. Marino S, Logan JG, Mellis D, Capulli M. Generation and culture of osteoclasts. BoneKEy Rep. 2014;3:570.
28. Song B, Haycraft CJ, Seo HS, Yoder BK, Serra R. Development of the post-natal growth plate requires intraflagellar transport proteins. Dev Biol. 2007;305(1):202–16.
29. de Andrea CE, Wiweger M, Prins F, Bovee JV, Romeo S, Hogendoorn PC. Primary cilia organization reflects polarity in the growth plate and implies loss of polarity and mosaicism in osteochondroma. Laboratory Investig. 2010;90(7):1091–101.
30. Pirog-Garcia KA, Meadows RS, Knowles L, et al. Reduced cell proliferation and increased apoptosis are significant pathological mechanisms in a murine model of mild pseudoachondroplasia resulting from a mutation in the C-terminal domain of COMP. Hum Mol Genet. 2007;16(17):2072–88.
31. Suleman F, Gualeni B, Gregson HJ, et al. A novel form of chondrocyte stress is triggered by a COMP mutation causing pseudoachondroplasia. Hum Mutat. 2012;33(1):218–31.
32. D'Angelo M, Yan Z, Nooreyazdan M, et al. MMP-13 is induced during chondrocyte hypertrophy. J Cell Biochem. 2000;77(4):678–93.
33. Wong M, Kireeva ML, Kolesnikova TV, Lau LF. Cyr61, product of a growth factor-inducible immediate-early gene, regulates chondrogenesis in mouse limb bud mesenchymal cells. Dev Biol. 1997;192(2):492–508.
34. Lee HH, Behringer RR. Conditional expression of Wnt4 during chondrogenesis leads to dwarfism in mice. PLoS One. 2007;2(5):e450.
35. Chang J, Sonoyama W, Wang Z, et al. Noncanonical Wnt-4 signaling enhances bone regeneration of mesenchymal stem cells in craniofacial defects through activation of p38 MAPK. J Biol Chem. 2007;282(42):30938–48.
36. Ma L, Wang HY. Mitogen-activated protein kinase p38 regulates the Wnt/cyclic GMP/Ca2+ non-canonical pathway. J Biol Chem. 2007;282(39):28980–90.
37. Oh CD, Chang SH, Yoon YM, et al. Opposing role of mitogen-activated protein kinase subtypes, erk-1/2 and p38, in the regulation of chondrogenesis of mesenchymes. J Biol Chem. 2000;275(8):5613–9.
38. Stanton L-A, Sabari S, Sampaio AV, Underhill TM, Beier F. p38 MAP kinase signalling is required for hypertrophic chondrocyte differentiation. Biochem J. 2004;378(Pt 1):53–62.
39. El Asmar Z, Terrand J, Jenty M, et al. Convergent signaling pathways controlled by LRP1 (receptor-related protein 1) cytoplasmic and extracellular domains limit cellular cholesterol accumulation. J Biol Chem. 2016;291(10):5116–27.
40. Suzuki A, Guicheux J, Palmer G, et al. Evidence for a role of p38 MAP kinase in expression of alkaline phosphatase during osteoblastic cell differentiation. Bone. 2002;30(1):91–8.
41. Hu Y, Chan E, Wang SX, Li B. Activation of p38 mitogen-activated protein kinase is required for osteoblast differentiation. Endocrinology. 2003;144(5):2068–74.
42. Hessler JL, Kreitman RJ. An early step in pseudomonas exotoxin action is removal of the terminal lysine residue, which allows binding to the KDEL receptor. Biochemistry. 1997;36(47):14577–82.
43. Konno K, Wakabayashi Y, Akashi-Takamura S, et al. A molecule that is associated with toll-like receptor 4 and regulates its cell surface expression. Biochem Biophys Res Commun. 2006;339(4):1076–82.
44. Hsieh JC, Lee L, Zhang L, et al. Mesd encodes an LRP5/6 chaperone essential for specification of mouse embryonic polarity. Cell. 2003;112(3):355–67.
45. Koduri V, Blacklow SC. Requirement for natively unstructured regions of mesoderm development candidate 2 in promoting low-density lipoprotein receptor-related protein 6 maturation. Biochemistry. 2007;46(22):6570–7.
46. Hoshi T, Tezuka T, Yokoyama K, Iemura S, Natsume T, Yamanashi Y. Mesdc2 plays a key role in cell-surface expression of Lrp4 and postsynaptic specialization in myotubes. FEBS Lett. 2013;587(23):3749–54.
47. D'Alessandro M, Richard M, Stigloher C, et al. CRELD1 is an evolutionarily-conserved maturational enhancer of ionotropic acetylcholine receptors. Elife. 2018;7:e39649.
48. Kawata K, Kubota S, Eguchi T, et al. Role of the low-density lipoprotein receptor-related protein-1 in regulation of chondrocyte differentiation. J Cell Physiol. 2010;222(1):138–48.
49. Worster AA, Nixon AJ, Brower-Toland BD, Williams J. Effect of transforming growth factor beta1 on chondrogenic differentiation of cultured equine mesenchymal stem cells. Am J Vet Res. 2000;61(9):1003–10.
50. Bartelt A, Behler-Janbeck F, Beil FT, et al. Lrp1 in osteoblasts controls osteoclast activity and protects against osteoporosis by limiting PDGF-RANKL signaling. Bone Res. 2018;6:4.
51. Lu D, Li J, Liu H, et al. LRP1 suppresses bone resorption in mice by inhibiting the RANKL-stimulated NF-kappaB and p38 pathways during osteoclastogenesis. J Bone Miner Res. 2018;33(10):1773–84.
52. Colwell AS, Krummel TM, Longaker MT, Lorenz HP. Wnt-4 expression is increased in fibroblasts after TGF-beta1 stimulation and during fetal and postnatal wound repair. Plast Reconstr Surg. 2006;117(7):2297–301.